https://doi.org/10.5194/egusphere-2026-1100
Preprint. Discussion started: 24 March 2026

Improving aerosol-radiation interaction feedback in AIRWISE operational system

Sumit Kumar[1,2], Gaurav Govardhan[1,3], Sreyashi Debnath[1,4], Avinash N. Parde[1], Sandeep Wagh[1], Jimy Dudhia[5], Sachin D. Ghude[1]

[1] Indian Institute of Tropical Meteorology, Pune, India

[2] Dept. of Atmospheric and Space Sciences, Savitribai Phule Pune University, Pune, India

[3] National Centre for Medium Range Weather Forecasting, Uttar Pradesh, India

[4] Dept. of Atmospheric and Oceanic Sciences, University of California, Los Angeles, United States

[5] National Center for Atmospheric Research, Boulder, United States

Correspondence to: Sumit Kumar (sr.sumit50@gmail.com)

Gaurav Govardhan (gaurav.govardhan@tropmet.res.in)

Abstract. Accurate representation of aerosol optical properties remains a key uncertainty in aerosol–radiation interactions in numerical weather prediction models, especially over highly polluted megacities. Operational systems use globally prescribed complex refractive indices (RIs) that inadequately represent regional aerosol composition, inducing biases in surface shortwave radiation (SWDOWN) and boundary layer evolution. In this study, region-specific RIs of aerosols over Delhi are implemented within the Air Quality Warning and Integrated Decision Support System for Emissions (AIRWISE) to quantify their radiative and meteorological impacts during the October 2023–January 2024 season. Sensitivity experiments with RIs of different chemical species indicate reduction in SWDOWN by up to ~80 W m^{-2} (diurnally ~43 W m^{-2}) during a severe post-monsoon episode. This radiative perturbation decreases surface temperature (~0.2 °C), near-surface wind speed (~0.4 m s^{-1}), and boundary layer height (~200 m), while increasing daytime humidity (3–4 %). Comparable sensitivity is observed during an extreme winter episode under stagnant, humid conditions favorable for haze persistence. Seasonally, monthly mean SWDOWN decreases by 25–37 W m^{-2} relative to the control simulation, accounting for ~¼ to ⅓ of total aerosol-induced reduction. Evaluation against surface radiation measurements from Winter Fog Experiment (WiFEX 2023–24) at Indira Gandhi International Airport, Delhi shows substantial bias reduction in December 2023 (62 %) and January 2024 (35 %). The revised radiative forcing systematically modifies near-surface thermodynamics and increases $PM_{2.5}$ concentrations, thereby altering pollution–meteorology feedback in highly polluted urban environments.

1 Introduction

Atmospheric aerosols play a crucial role in modulating the earth's radiation budget (Haywood and Shine, 1995; Kim and Ramanathan, 2008), influencing the hydrological cycle (rainfall, glacier and snow melt) and shaping regional climate

https://doi.org/10.5194/egusphere-2026-1100
Preprint. Discussion started: 24 March 2026

dynamics (Seinfeld et al., 2016; Bellouin et al., 2020). Beyond their impact on weather, aerosols also affect daily life by deteriorating air quality (Tomasi et al., 2016) and reducing visibility during foggy conditions, leading to socioeconomic and health consequences (Ghude et al., 2017, 2023). The atmospheric residence time of aerosols is a critical factor in modulating weather and climate systems, as their prolonged presence alters radiative transfer processes and atmospheric thermodynamics. In regions with severe air pollution, such as those affected by post-monsoon stubble burning in India (Govardhan et al., 2023) or wintertime shallow boundary layers in northern India (Ghude et al., 2023), aerosol-induced changes in radiation fluxes can substantially modify local meteorological variables and air quality. These aerosol–radiation–meteorology feedback are also critical for operational air quality forecasting over polluted megacities (Ghude et al., 2024). The operational systems such as the Air Quality Warning and Integrated Decision Support System for Emissions (AIRWISE) demonstrate that deficiencies in aerosol representation and aerosol–radiation coupling can directly limit the prediction of extreme wintertime pollution episodes.

Aerosol–radiation interactions (ARI) are represented in numerical weather prediction (NWP) and climate models through various radiation parameterization schemes. Among the widely used schemes, the Rapid Radiative Transfer Model for Global Models (RRTMG) (Iacono et al., 2008), Community Radiative Transfer Model (CRTM) (Han, 2006), Goddard (Chou and Suarez, 1999), and the Community Atmosphere Model (CAM) (Collins et al., 2004) provide robust frameworks for simulating aerosol-induced modifications in radiation fluxes. Within these models, Mie scattering plays a fundamental role in deriving aerosol optical properties incorporating an assumed size distribution and complex refractive index (RI), which directly influence radiative transfer processes. The shortwave radiation reaching the Earth's surface serves as a primary heating agent for the atmosphere (Lettau and Lettau, 1969). This radiative heating perturbs the near-surface air mass, affecting key meteorological variables such as temperature, wind speed, relative humidity and, thereby influencing atmospheric physical processes such as convection and turbulence (Li et al., 2017; Bender et al., 2020). The dispersion of pollutants within the planetary boundary layer height (PBLH) is strongly modulated by wind and turbulence (Govardhan et al., 2015).

Understanding aerosol feedback mechanisms is crucial for improving meteorological predictions and regulating extreme pollution events. Aerosols significantly influence radiative forcing (Ramanathan et al., 2001), boundary layer dynamics, and pollutant dispersion (Yu et al., 2002), making their accurate representation in NWP models essential for better air quality forecasts and climate assessments. The role of aerosols in cloud microphysics and radiative interactions has long been recognized (Twomey, 1977), highlighting their impact on climate forcing and regional weather patterns. For instance, a mean bias of 34 W m^{-2} in downwelling shortwave radiation and a warm bias of 3 °C in surface temperature were documented while simulating high-aerosol events over Delhi during the winter season of 2020–2021 by Sengupta et al., 2022. Such biases in shortwave radiation have also been reported over multiple regions globally (Wild, 2005; Ruiz-Arias et al., 2016). The discrepancies in simulated shortwave radiation directly affect the interaction with prescribed aerosol species

https://doi.org/10.5194/egusphere-2026-1100
Preprint. Discussion started: 24 March 2026

in the WRF-Chem, introducing uncertainties in surface energy balance estimations. Moreover, disturbances in the surface energy budget can lead to unrealistic radiative forcing (Stier et al., 2013), with the magnitude and sign of the forcing depending on whether the bias in radiation is positive or negative. Addressing these uncertainties is essential for improving the fidelity of ARIs in NWP models

Key aerosol optical properties such as aerosol optical depth (AOD), single scattering albedo (SSA), and asymmetry factor (AF), determine the extent of solar radiation absorption and scattering, directly affecting local surface radiation fluxes, particularly during daytime when shortwave radiation dominates. These properties are formulated in the model as a function of wavelength and position vector of the particle (Ghan et al., 2001). In the WRF-Chem model, these properties are parameterized within the chemistry section, with calculations performed across four shortwave radiation bands (centered at 300, 400, 600, and 999 nm) and sixteen longwave radiation bands (Fast et al., 2006; Barnard et al., 2010). The AOD at specific wavelengths, such as 400 and 600 nm, is derived using the Ångström exponent formula, enabling interpolation to other wavelengths within the shortwave spectrum (Zhao et al., 2013). Similarly, SSA and AF values are computed and subsequently interpolated for different spectral bands to refine their representation in radiation schemes. The RI values of aerosol particles play a fundamental role in determining their radiative properties, influencing both absorption and scattering processes. The scattering and absorption cross-sections of aerosols are primarily dictated by their complex RIs and morphological characteristics, including shape and size (Bond and Bergstrom, 2006).

The RI values of the aerosol species, such as contributing to $PM_{2.5}$, affect the surface radiation fluxes. Among mineral dust components, hematite (Fe_2O_3) is a key absorber (Sokolik and Toon, 1999; Lafon et al., 2006; Koven and Fung, 2006), with a global average of 6.85 % (Goudie, 1978), though its concentration varies from 0–4 % in the Thar Desert (Negi et al., 1996, 2002). Notably, Kukas Hill near Jaipur exhibits an exceptionally high hematite content of 42.82 % (Agnihotri et al., 2015). Morphological studies using Scanning Electron Microscopy identified mineral dust shapes as spheres, spheroids, chebyshev, and cylinders (Mishra and Tripathi, 2008), with sensitivity experiments showing RI values of dust decrease with wavelength. Balloon-based observations over Delhi (Mishra et al., 2018) further revealed higher hematite concentrations (~4 %) near the surface, reinforcing the need to revise dust RI values in NWP models, where they are often treated as constants.

Furthermore, the complex RI of Black Carbon (BC) in NWP models has been a subject of ongoing debate. The wavelength-dependent RI values were derived by Chang and Charalampopoulos (1990) based on experimental measurements of propane-air flame soot particles. However, an alternative approach by Bond and Bergstrom (2006) suggested a constant RI value of 1.95 + 0.79i at 0.55 µm for light-absorbing carbon (LAC), a specialized term for BC across the entire shortwave spectrum. This value was obtained through an extrapolation process that intersected an imaginary upper void-fraction line for experimentally derived RI values of non-graphite LAC with a graphitization line. However, this prescribed RI was not directly supported by experimental data and was found to underpredict the measured mass absorption cross-section for uncoated BC aggregates at 0.55 µm by approximately 30 % (Liu et al., 2020). A more recent study by

https://doi.org/10.5194/egusphere-2026-1100
Preprint. Discussion started: 24 March 2026

Moteki et al. (2023) incorporated aggregate shape and size effects of BC and employed the complex scattering amplitude sensing technique to individually characterize water-insoluble BC particles. Using Bayesian data analysis, the study derived the distributed complex scattering amplitude of waterborne BC particles and recommended an updated RI value of 1.95 + 0.96i. This value reflects a 0.17 increase in the imaginary component compared to those used in current aerosol-climate models, leading to improved agreement with observed BC absorption characteristics.

Regarding organic carbon (OC), it has generally been assumed to function purely as a scattering aerosol (Kanakidou et al., 2005), with a zero imaginary component of RI prescribed in NWP models. However, Kirchstetter and Novakov (2004) provided evidence that a subset of OC exhibits wavelength-dependent absorption, particularly in the ultraviolet and visible spectral regions, based on filter-based measurements of biomass combustion and motor vehicle emissions. Other studies (Graber and Rudich, 2006; Adler et al., 2010; Chen and Bond, 2010; Kim et al., 2012) have also mentioned that OC containing aerosol shows the light absorption near low wavelength spectral range.

Sulfate aerosols, primarily composed of ammonium sulfate, are considered scattering aerosols in the atmosphere. The imaginary part of the RI for uncoated sulfate aerosols is approximately 10^{-7} at 0.55 µm (Toon et al., 1976; Hess et al., 1998), and this value has been accurately implemented in NWP models irrespective of the region. In addition to sulfate, sea-salt aerosols, predominantly composed of sodium chloride, play a significant role in coastal regions, especially when mixed with organic aerosols. The imaginary component of RI for sea-salt is approximately 10^{-9} in the visible spectral range (Shettle and Fenn, 1979), indicating negligible absorption. Its concentration, however, is minimal over continental surfaces, where other aerosol species dominate.

Therefore, default RI values implemented in current NWP models may not be suitable for region-specific studies, potentially limiting the accuracy of ARI in localized air quality and climate assessments. In this study, we incorporate region-specific aerosol optical properties, particularly over the urban region of Delhi, as a function of observed or calculated RI values in the AIRWISE model setup. Furthermore, we assess the impact of aerosol optical properties on surface meteorology and air pollution, quantifying biases from October 2023 to January 2024 using the WRF-Chem model. The data and methodology are detailed in Sect. 2, results are presented in Sect. 3, key findings are discussed in Sect. 4, and overall conclusions are provided in the final section.

2 Data and Methodology

2.1 Model description and configuration

WRF-Chem is a fully coupled, online chemistry transport model that integrates atmospheric chemistry and aerosol processes within the Advanced Research WRF framework (Skamarock et al., 2019), allowing for direct interactions between meteorology and atmospheric composition. Unlike offline chemical transport models, WRF-Chem simultaneously simulates

https://doi.org/10.5194/egusphere-2026-1100
Preprint. Discussion started: 24 March 2026

the evolution of weather and chemical constituents, enabling a more accurate representation of feedback mechanisms between aerosols, radiation, and clouds (Grell et al., 2005). This capability makes it a powerful tool for studying air quality, regional and urban-scale pollution, and the climatic impacts of anthropogenic and natural emissions. The model supports multiple chemical mechanisms and includes various aerosol schemes to simulate secondary organic aerosols, BC, dust, and sea salt (Emmons et al., 2010; Zaveri et al., 2008). The model offers a wide range of dynamical and chemical parameterizations, with multiple physics options, including microphysics, radiation, and planetary boundary layer schemes, tailored to different geographical regions and atmospheric conditions (Powers et al., 2017; Zhang, 2008). Additionally, its fully coupled online feedback mechanisms allow for detailed simulations of aerosol-cloud-radiation interactions, capturing the direct and indirect effects of aerosols on weather and climate (Saide et al., 2012; Baklanov et al., 2014; Glotfelty et al., 2019). These capabilities make WRF-Chem a crucial tool for assessing the impacts of emissions on atmospheric processes.

We adopt the same core WRF-Chem (v.3.9.1) (Skamarock et al., 2008) model setup and configuration as used in the operational AIRWISE system (Ghude et al., 2020; Kumar et al., 2020; Jena et al., 2021). The study region, depicted in Fig. S1 (in supplement), is centered over Delhi (28.7° N, 77.5° E) and consists of two nested domains (d01 and d02). The outer domain (d01) encompasses North India, extending from 62° E to 93° E and 21° N to 36° N, with a horizontal resolution of 10 km × 10 km and a grid size of 300 × 170 points. The inner domain (d02) focuses on Delhi and the National Capital Region (NCR), covering an area from 75° E to 78° E and 26° N to 30° N, with a higher resolution of 2 km × 2 km and a grid size of 161 × 201 points. Each domain consists of 50 vertical levels, with 8 levels within the first kilometres from the surface, and the model top is set at 50 hPa. To focus on urbanized regions, such as Delhi, the output from both domains (d01 and d02) has been masked to represent Delhi specifically. Simulations were conducted in the period from September 2023 to January 2024 capturing the high aerosol loading during the stubble burning season (mid-October to November) and the winter period in the study region. The physics schemes used in the model simulations include several key components designed to accurately represent various atmospheric processes. The WRF Single-Moment 6-class (WSM6) scheme is employed for microphysics, which simulates cloud processes (including cloud water, rain, snow, and ice) based on a single moment approach (Hong and Lim, 2006). Longwave and shortwave radiation is handled by the RRTMG, which provides efficient and accurate computation of radiative transfer and detailed representation of the solar radiation absorbed and scattered by the atmosphere (Mlawer et al., 1997; Iacono et al., 2008). The boundary-layer physics are represented by the Mellor-Yamada Nakanishi and Niino 2.5 level (MYNN 2.5) scheme, which is designed to model turbulent mixing and the vertical structure of the boundary layer (Nakanishi and Niino, 2004). For convective parameterization, the Grell-Freitas Ensemble scheme is used, for its ability to represent deep convection and its interaction with larger-scale weather systems (Grell and Freitas, 2014). The Unified Noah Land-Surface Model is utilized to simulate land-surface interactions, including the exchange of heat, moisture, and momentum between the surface and the atmosphere (Chen and Dudhia, 2001). Finally, the Eta Similarity scheme is applied in the surface layer, providing near-surface turbulent fluxes based on atmospheric stability (Businger et al., 1971). These configurations of the physics schemes have been summarized in Table S1.

https://doi.org/10.5194/egusphere-2026-1100
Preprint. Discussion started: 24 March 2026

2.1.1 Meteorological boundary conditions

The 6-hourly meteorological datasets from the European Centre for Medium-Range Weather Forecast (ECMWF) reanalysis (ERA5) were utilized to generate the initial and boundary conditions for the domain d01. These datasets, with a horizontal resolution of 0.25° × 0.25°, provide comprehensive information on various meteorological variables such as temperature, pressure, humidity, wind speed, and wind direction (Hersbach et al., 2020), which are essential for initializing the model simulations. The ERA5 data were used to define the conditions at the boundaries of the domain d01, and the model output from d01 was subsequently downscaled to provide the boundary conditions for the domain d02, which covers a smaller region with a higher resolution. For geographical data, including terrestrial and land-use information, the stationary datasets are interpolated from the Moderate Resolution Imaging Spectroradiometer (MODIS) International Geosphere-Biosphere Programme (IGBP) 21-category land-cover classification datasets (Friedl et al., 2002). These datasets were mapped onto the model grid points to represent land-use types and surface properties such as vegetation, water bodies, and urban areas, which influence surface energy exchanges and other meteorological processes. The interpolation ensures that the land-use data are appropriately matched to the finer resolution of the model grid, particularly for the domain d02.

2.1.2 Chemistry formulation: Emissions, boundary conditions, and mechanism

The monthly anthropogenic emissions of aerosols were derived from the Emission Database for Global Atmospheric Hemispheric Transport of Air Pollutants version 2.2 (EDGAR-HTAPv2.2), which provides datasets from 2010 at a horizontal resolution of 0.1° × 0.1° (Janssens-Maenhout et al., 2015). This global inventory includes sector-specific emissions, such as those from transportation, industrial activities, power and energy generation, residential sources, and agriculture. For this study, anthropogenic emissions were further refined by incorporating fine-gridded emissions data over Delhi-NCR region. For biomass burning and prescribed fire emissions, hourly temporal data at a 1 km spatial resolution were obtained from the Fire Inventory from NCAR version 2.5 (FINNv2.5) (Wiedinmyer et al., 2011). The biogenic emissions during the study period were incorporated using the Model of Emissions of Gases and Aerosol from Nature version 2.0 (MEGANv2.0), which estimates emissions from natural sources such as vegetation (Guenther et al., 2006).

The chemical boundary conditions for the domain d01 were set using the Model for Ozone and Related Tracers version 4 (MOZART-4), which provides chemical climatological data for the study region (Emmons et al., 2010). The gas-phase chemistry was simulated using the chemical mechanisms from this global chemical transport model. Additionally, the Goddard Chemistry Aerosol Radiation and Transport (GOCART) model was employed to simulate aerosol chemistry and related processes, including transportation, deposition, nucleation, and accumulation (Chin et al., 2000). GOCART tracks aerosol species like BC, OC, and sulfate as bulk aerosol species, while dust and sea-salt are resolved in five and four size bins, respectively, for more accurate representation of their distribution and behavior in the atmosphere.

https://doi.org/10.5194/egusphere-2026-1100
Preprint. Discussion started: 24 March 2026

2.2 Experiment details

In the WRF-Chem model, the $PM_{2.5}$ is composed of several aerosol species, including hydrophobic and hydrophilic BC (BC1 and BC2), hydrophobic and hydrophilic OC (OC1 and OC2), Dust with two size bins (Dust1 and Dust2, with effective radii of 0.5 µm and 1.4 µm, respectively), Sea-Salt with two size bins (SEAS1 and SEAS2, with effective radii of 0.3 µm and 1.0 µm, respectively), Sulfate, and other GOCART primary $PM_{2.5}$ (i.e., P25) (Govardhan et al., 2023). The optical properties of these aerosol species, including their scattering and absorption cross-sections, are separately computed in the model. These properties depend primarily on the complex RI and the morphology (shape and size) of the aerosols (Barnard et al., 2010; Tuccella et al., 2015). These RIs are basically used in the calculation of optical properties of the aerosols (such as SSA, AF etc.) using 3 methods: (a) Volume averaging mixing rule, (b) Maxwell-Garnett mixing rule and, (c) Shell-core method in the WRF-Chem model. For this study we have used the volume averaging mixing rule for the calculation of optical properties keeping in mind the mixing state of aerosols in the ambient environment of Delhi (Srivastava et al., 2017). The detailed explanation of these rules can be found in the literature (Fast et al., 2006; Barnard et al., 2010). The optical properties are then used in the Mie subroutines to solve the radiative transfer equations in the model. The full Mie calculations are computationally expensive in the sense that they solve each equation separately and hence require more time for the model to simulate radiative transfer fluxes. An alternate subroutine that is computationally fast, but can be less accurate, uses the Chebyshev economization method (detailed explanation in Ghan et al., 2001) for the calculation of radiative fluxes. The downwelling shortwave radiation at the ground level of the model is then produced after interacting with various entities present in the atmosphere. Hence, inaccurate prescription of aerosol optical parameters can lead to erroneous simulations of their radiation interactions (Haywood and Boucher, 2000).

To improve the accuracy of aerosol-radiation interactions in our study region, the RIs of Dust, BC, OC, and P25 were modified in the model. The values of complex RIs used in the study for the aerosol species were obtained from the available literature. These values were either region specific, calculated using the sampling techniques or laboratory tested values calculated under the controlled environment which may be valid for any region of interest. The details of the modified complex refractive indices are summarized in Table 1.

Table 1. Original and modified values of the complex refractive indices of aerosol species employed in the WRF-Chem model.

S. No.	Aerosol Species	Wavelength (um)	Original values of Refractive Indices		Modified values of Refractive Indices		References
			Real Part (n)	Imaginary Part (k)	Real Part (n)	Imaginary Part (k)	
1.	**Dust**	0.30			1.565	0.0500	Mishra and

https://doi.org/10.5194/egusphere-2026-1100
Preprint. Discussion started: 24 March 2026

		0.40 0.60 1.00	1.550	0.003	1.573 1.565 1.548	0.0280 0.0035 0.0005	Tripathi, 2008
2.	**Black Carbon (BC)**	0.30 0.40 0.60 1.00	1.95	0.79	1.95	0.96	Moteki et al., 2023
3.	**Organic Carbon (OC)**	0.30 0.40 0.60 1.00	1.45	0.00	1.45 1.45 1.45 1.45	0.249 0.109 0.017 0.000	Kirchstetter et al., 2004
4.	**Other GOCART Primary $PM_{2.5}$ (P25)**	0.30 0.40 0.60 1.00	1.550	0.003	1.565 1.573 1.565 1.548	0.0500 0.0280 0.0035 0.0005	Mishra and Tripathi, 2008

The original values of the RI were found to be independent of wavelength in WRF-Chem i.e., these species can scatter (real part of RI) and absorb (imaginary part of RI) the radiation with the same factor for all the 4 shortwave radiation bands present in the model. However, in the literature it was found that the RI values of these species depend on wavelength (except BC) and have different scattering or absorbing nature in each shortwave radiation band. Furthermore, OC was assumed to be non-absorbing in the model, but literature suggests an imaginary part of RI at few shortwave radiation bands (Table 1). The real part of RI values prescribed in the model for all the species mentioned above are approximately in agreement with the literature. However, the imaginary parts differ. Our modifications RI, thus make the model aerosol mixture more absorbing.

Eight experiments were conducted to assess the impact of ARI under various conditions. Among these, three experiments were designed to evaluate which radiation scheme, namely RRTMG, Goddard, or CAM, produces surface fluxes most consistent with observations. To isolate the role of aerosol–radiation feedback, EXP1 was performed with the aerosol-radiation feedback turned off. Additionally, four experiments (EXP2 to EXP5) were carried out to investigate the individual contributions of specific chemical species to the shortwave radiation reaching the surface. A summary of all experiments is provided in Table 2.

Table 2. Summary of the experiments performed

S.	Experiment name	Details

https://doi.org/10.5194/egusphere-2026-1100
Preprint. Discussion started: 24 March 2026

No.		
1.	RRTMG (or CTRL)	Radiation parameterization with RRTMG
2.	Goddard	Radiation parameterization with Goddard
3.	CAM	Radiation parameterization with CAM
4.	EXP1 (No-Feedback)	No aerosol-radiation feedback
5.	EXP2 (Dust)	Modified refractive index of Dust only
6.	EXP3 (BC)	Modified refractive index of BC only
7.	EXP4 (OC)	Modified refractive index of OC only
8.	EXP5 (All-Species)	Modified refractive index of Dust, BC, OC, and P25

To examine the impacts of modifications in the optical properties of aerosols on the downwelling shortwave radiation in the WRF-Chem, we chose extreme pollution events that occurred in Delhi 2023-24. Figure 1 presents the mean observed $PM_{2.5}$ concentrations recorded over Delhi from 20 September 2023 to 31 January 2024. During this period, concentrations peaked at ~565 µg m^{-3}, primarily due to local emissions from firecrackers burning on the eve of the Diwali festival. To evaluate the impact of modified aerosol optical properties in the model, two special case studies were designed to represent periods of high aerosol loading: (a) a post-monsoon episode and (b) a typical winter event over Delhi.

The first case (Event-I), covers a 10-day period from 1 to 10 November 2023, chosen to represent intense aerosol loading due to enhanced anthropogenic activity and widespread crop residue burning in neighbouring states. During this event, $PM_{2.5}$ concentrations reached as high as 500 µg m^{-3}, with some days recording around 400 µg m^{-3} (Fig. 1). Daytime concentrations typically ranged between 200–300 µg m^{-3}. The second case (Event-II), spanning from 8 to 18 January 2024, was selected to investigate the influence of the modified optical properties under winter meteorological conditions characterized by low temperatures, high relative humidity, and stagnant wind patterns. This event was marked by persistent fog and low-level clouds that significantly diminished incoming solar radiation. $PM_{2.5}$ concentrations during this period peaked at ~550 µg m^{-3}, with values on most days ranging between ~100 to 300 µg m^{-3}.

https://doi.org/10.5194/egusphere-2026-1100
Preprint. Discussion started: 24 March 2026

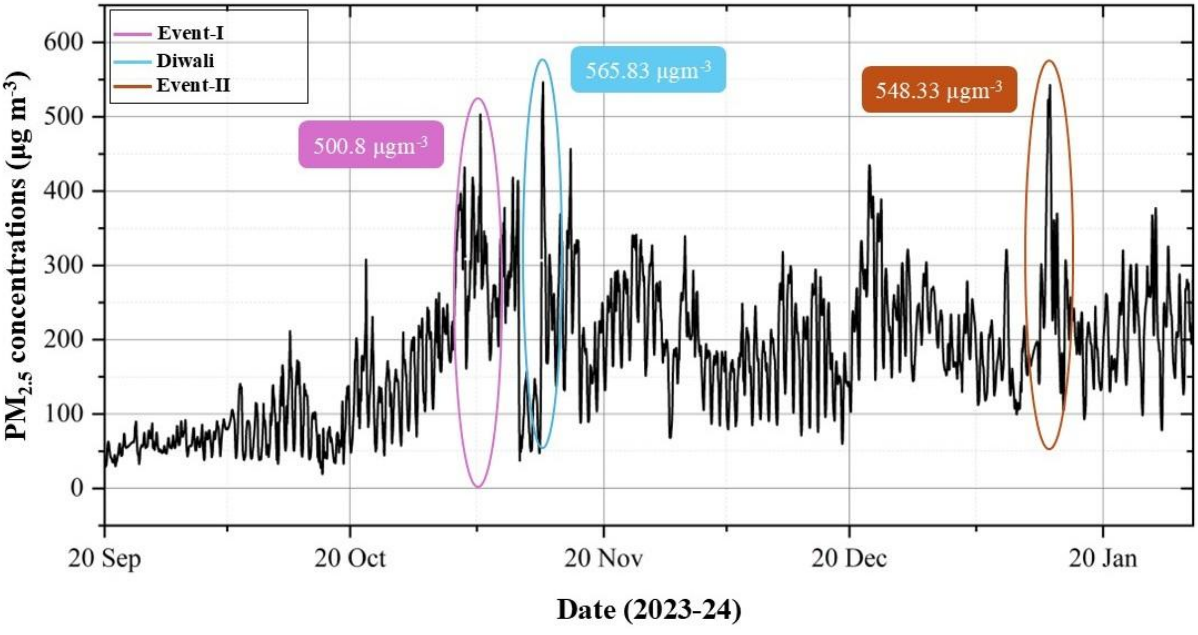

Fig. 1. Ground based $PM_{2.5}$ measurements over Delhi for the period between 20 September 2023 to 31 January 2024.

For these high pollution events (Event-I and Event-II), a spin-up time of two days was applied for each simulation to ensure model stability. Also, the comparison of these experiments was carried out for the outer domain (d01) with the observations to understand the regional impacts and variations in ARI.

The same set of experiments (EXP1 to EXP5) was also conducted for the period from 20 September 2023 to 31 January 2024, with a 10-day spin-up, over domains d01 and d02. This long-term four-month simulation was designed to examine the impacts of modified aerosol optical properties on downwelling shortwave radiation (hereafter SWDOWN) over an extended period and during non-episodic pollution conditions. The results were analysed under both all-sky conditions (atmosphere with clouds, aerosols, trace gases etc.) and clear-sky conditions (atmosphere without clouds). For the clear-sky analysis, all data points influenced by cloud cover were excluded by retaining only those grid points and time steps with a cloud fraction less than 0.1 at all models' vertical levels.

2.3 Observational datasets

2.3.1 Radiation and meteorological data

The quality-controlled observational datasets used for the comparison of model simulations include downwelling shortwave radiation measurements from a net radiometer, along with meteorological variables such as temperature at 2 m (T2), relative humidity at 2 m (RH2), and wind speed at 10 m (WS10). These data were collected using integrated smart

https://doi.org/10.5194/egusphere-2026-1100
Preprint. Discussion started: 24 March 2026

weather sensors mounted on a 20 m micro-meteorological tower during the Winter Fog Experiment (WiFEX) campaign, which took place from 2023 to 2024 at Indira Gandhi International (IGI) Airport, Delhi. A ceilometer attenuated backscatter data was used to identify and separate cloudy and foggy hours datasets in both surface observations and simulations. To ensure the integrity and quality of the datasets, a series of data quality control steps were undertaken. Any missing or negative values in the datasets were addressed and corrected before further analysis. Additionally, days with less than 40 % of valid measurements were excluded from the dataset to eliminate potential errors associated with malfunctioning or incomplete sensor data, ensuring the reliability of the comparison. This cleaning process helped mitigate biases that could result from faulty measurements and ensured that only high-quality, reliable data were used in the evaluation. Furthermore, since the sensors recorded data on a per-minute basis, but the model simulations provided hourly output, the observational data were averaged over each hour to match the model's temporal resolution.

2.3.2 $PM_{2.5}$ concentrations data

The ground-based hourly mass concentrations of $PM_{2.5}$, collected by the Central Pollution Control Board (CPCB) and Delhi Pollution Control Committee (DPCC) at 40 monitoring stations across Delhi (Sengupta et al., 2022), were used to evaluate the model-simulated $PM_{2.5}$ concentrations for the study region. The CPCB and DPCC follows stringent quality control procedures to ensure the accuracy and reliability of the air quality data. These datasets offer a comprehensive representation of $PM_{2.5}$ concentrations at various locations across the city and serve as a benchmark for comparing the model outputs. Before using the data for comparison with the model, the datasets underwent thorough quality checks. Any missing, erroneous, or zero values were identified and rectified to avoid introducing biases into the analysis. This was particularly important to ensure the accuracy of the comparison, as gaps or anomalies in the observational data could lead to misleading conclusions about the model's performance. In addition, days with significant data gaps or sensor malfunctions were excluded to enhance the reliability of the evaluation. The utilization of this ground-based dataset allowed for a detailed comparison between the observed $PM_{2.5}$ concentrations and the model-simulated values, offering insights into the model's ability to replicate observed air quality patterns. This comparison is crucial for evaluating the model's performance in capturing $PM_{2.5}$ pollution, particularly in an urban setting like Delhi, where factors such as vehicular emissions, industrial activity, and seasonal variations significantly influence air quality.

2.4 Statistical evaluation

The comparison of model-simulated meteorological variables (SWDOWN, T2, RH2, WS10), and mass concentrations of $PM_{2.5}$ with observational datasets was carried out using various statistical parameters to assess the model's performance. These parameters included Mean Bias (MB), Root Mean Square Error (RMSE), Normalized Mean Square Error (NMSE), and Fractional Bias (FB). These statistical metrics offer a comprehensive evaluation of how well the model simulations align with the observed datasets. The detailed formulas and descriptions for each of these statistical parameters are provided in the supplement (Table S2).

https://doi.org/10.5194/egusphere-2026-1100
Preprint. Discussion started: 24 March 2026

3 Results

3.1 Choice of shortwave radiation parameterization scheme

To choose the best amongst multiple shortwave radiation parameterization schemes available in WRF-Chem, we ran the model with the default optical properties of aerosols with three different schemes. We chose RRTMG, Goddard and CAM for this exercise and compared the diurnal cycles of averaged SWDOWN simulated over Delhi using these schemes with the corresponding observations. The comparisons are done for the month of December 2023 under clear-sky conditions in which we have removed the cloud cover (set > 0.1) in the model along with the foggy hours by utilizing the ceilometer backscatter (Fig. 2). It can be seen that, in comparison with RRTMG, the simulated SWDOWN in Goddard and CAM, overestimate the observations. Overall, all the radiation schemes overestimate SWDOWN during the morning hours (0:00 to 12:00 LT), but Goddard and CAM, overestimate SWDOWN throughout the day, while RRTMG shows a closer match to the observed values especially during the afternoon hours.

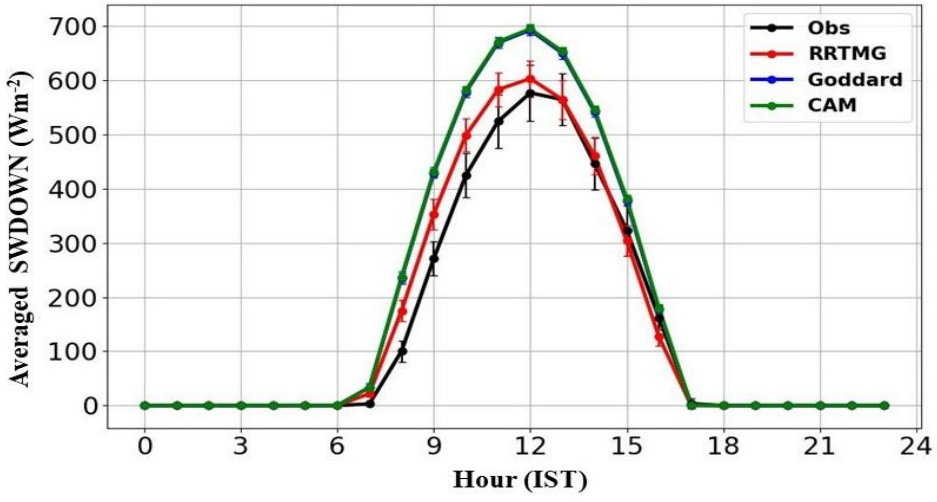

Fig. 2. Diurnal cycle of simulated SWDOWN by different schemes: RRTMG, Goddard, CAM with observations in the month of December 2023 (monthly mean) over Delhi. IST refers to the Indian Standard Time i.e. Local Time (LT).

The biases between Goddard and CAM are roughly at least twice or even more of those for RRTMG (Table S3). In fact, RRTMG shows a very good agreement with the observations during the mid-day hours of 12:00–15:00 LT. The maximum differences in the model schemes and the observations occur around 09:00 LT, while the minima for RRTMG comes at 13:00 LT and that for Goddard and CAM is reached at 17:00 LT. Thus, RRTMG is found to be more accurate in capturing the SWDOWN vis-a-vis the other available radiation parameterization schemes. Therefore, we choose the RRTMG scheme to parameterize the shortwave radiative processes in the further experiments of this study. We refer to this configuration as CTRL in the next sections.

https://doi.org/10.5194/egusphere-2026-1100
Preprint. Discussion started: 24 March 2026

3.2 Impacts of modified aerosol optical properties on surface shortwave radiation

As mentioned in Sect. 2.2, we examine the impacts of modified aerosol optical properties on the SWDOWN for the two extreme pollution cases. The simulated near-surface $PM_{2.5}$ mass concentration for both these events are shown in Fig. S2. Since, we are analysing the impacts of the modified aerosol optical properties on SWDOWN mainly in clear-sky conditions, here, we show the comparison of modelled $PM_{2.5}$ with the observations in the clear-sky. For Event-I i.e., 1 to 10 November 2023 (Fig. S2a), the observations depict a peak in $PM_{2.5}$ mass concentrations during the afternoon hours of 5 November, and the values go beyond 500 μg m^{-3}. The model in the CTRL configuration rises a little up to 400 μg m^{-3}, capturing the signature of the peak, but failing to capture the exact magnitude. On the contrary, during the afternoon hours of 4 November, the observations just manage to cross 400 μg m^{-3}, but the CTRL simulations reach beyond 450 μg m^{-3}. For all the other days, the CTRL configuration captures observed tendency of the $PM_{2.5}$, even the values also are seen to be within ± 20 % of the observations. However, on the 6 and 7 November, the model shows an overestimation in comparison with observations. This is likely related to the uncertain biomass burning emissions from fires mainly from the neighbouring states of Punjab and Haryana. To confirm this, we have done more simulation in CTRL configuration without the prescription of biomass burning emissions. The modelled $PM_{2.5}$ in that configuration (Fig. S3) can be seen to reduce down especially on 6 and 7 November, thus highlighting the role played by fire emissions in causing the large disagreements between model and observations on those days. Overall, the CTRL configuration fails to capture the exact magnitude of the observed $PM_{2.5}$, but the signals of the extreme pollution are well captured with $PM_{2.5}$ magnitudes not too low vis-a-vis observations.

For Event-II of extreme pollution i.e. from 8 to 18 January 2024 (Fig. S2b), most of the days are mainly affected by dense fog spells (Kant et al., 2025), especially up to 14 January. This is partly related to the inability of the model to capture foggy conditions due to a bias in RH (Sengupta et al., 2022), and consequently the underestimated hygroscopic growth of aerosols in the model, which limits the magnitude of simulated $PM_{2.5}$. Nevertheless, the model fairly captures the signals of the observed $PM_{2.5}$ under clear-sky conditions, though the exact values are missed. Thus, for both the events, the model in CTRL configuration captures the observed signatures of peak signals, however the peak magnitudes are missed. Nevertheless, the model's atmosphere has enough ambient aerosols under clear-sky conditions, to interact with the incoming shortwave radiation and show impacts of the modified optical properties on it.

We now evaluate the simulated SWDOWN in the CTRL and EXP5 configuration which is the combined modified RIs of all chemical species and compare it with the corresponding observational data at the WiFEX site. Due to unavailability of data during the Event-I of high Air Quality Index (AQI) (i.e. during November 2023), we have done the model-observation comparisons only for Event-II i.e. during 8 to 18 January 2024 (Fig. 3a). It may be noted that the comparisons are done only for the cloud- and fog-free scenarios. This results in screening-out of most of the early morning data. The simulated SWDOWN shows a satisfactory comparison with the observations by capturing the day-to-day variation in high and lows, however the magnitudes differ substantially. The EXP5 (All-Species) configuration tends to reduce the

https://doi.org/10.5194/egusphere-2026-1100
Preprint. Discussion started: 24 March 2026

SWDOWN in comparison with CTRL. The bias in the SWDOWN reduces by around 10-15 W m^{-2} especially from 10–12 January (Fig. 3b). Towards latter half of the study period (14–18 January), the bias vis-a-vis observations in fact increases by as high as 25 W m^{-2}. In general, the EXP5 configuration reduces the downwelling shortwave radiation at the surface by 10 – 25 W m^{-2}. The MB, RMSE, NMSE, and the FB are 4.58 (0.86) W m^{-2}, 22.45 (21.61) W m^{-2}, 0.043 (0.042), and 0.042 (0.008) for the CTRL (EXP5) experiment (Table S5). Thus, the deviations of the simulated SWDOWN from the observations are reduced substantially upon modifying the optical properties of the aerosols.

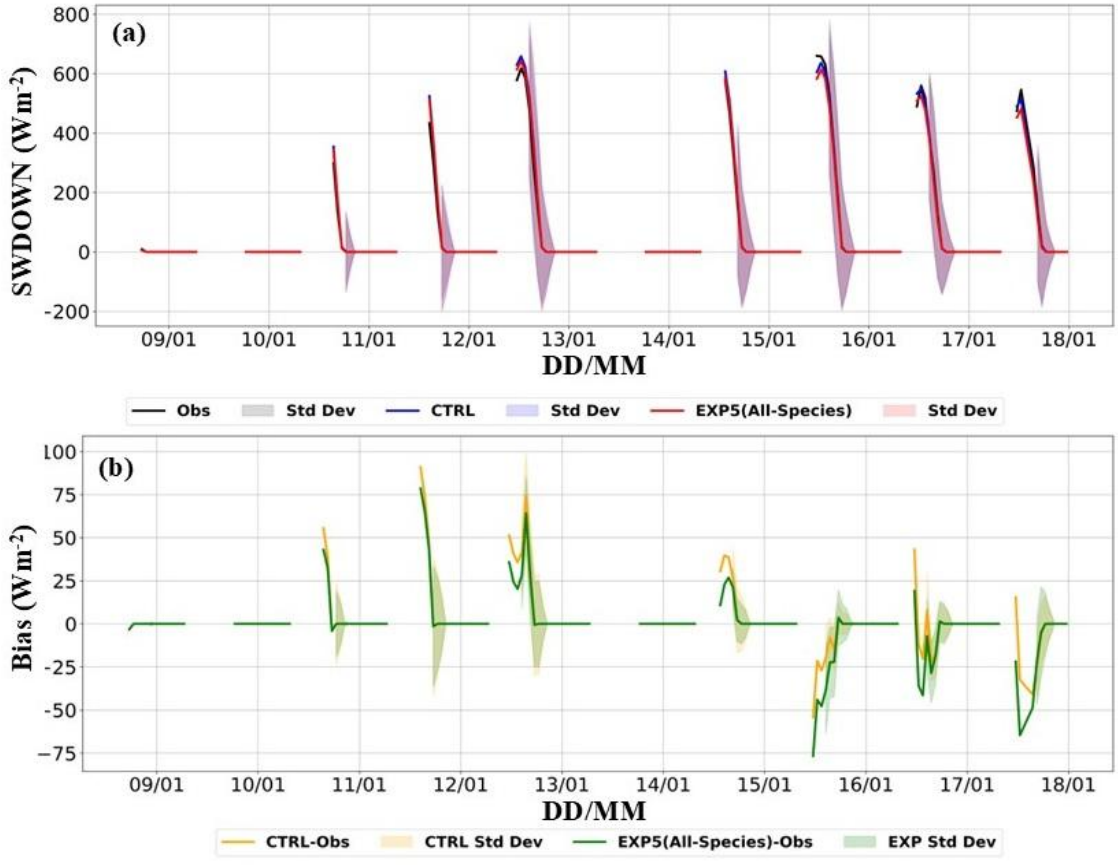

Fig. 3. (a) Time series of simulated SWDOWN in CTRL and EXP5 along with observations over Delhi, and (b) bias in CTRL and EXP5 configurations during Event-II.

To isolate the impacts of the modifications in the individual aerosol species' optical properties in causing such changes in SWDOWN, we plot the hourly difference in clear-sky SWDOWN in each of the sensitivity experiments vis-a-vis the CTRL configuration in Fig. 4a (for Event-I) and 4b (for Event-II), the event-mean hourly differences in the SWDOWN are plotted in Figs. 4c and 4d for Event-I and the Event-II respectively. Additionally, the total impacts of ARI on the

https://doi.org/10.5194/egusphere-2026-1100
Preprint. Discussion started: 24 March 2026

SWDOWN have also been computed as the difference between the EXP1(No-feedback) and CTRL configuration. Those values have also been plotted in hourly as well as season-mean hourly basis in Figs. 4a–4d. It may be seen that the hourly changes in SWDOWN due to the modified optical properties of all aerosol species could go as high as 80 W m^{-2} on the polluted days of the 7 and the 8 of November (Fig. 4a). These changes are roughly (⅓)rd of the total clear-sky aerosol radiation impact on the given day. On the contrary, during the winter month of January 2024, the corresponding changes on the extreme pollution days are around 30-40 W m^{-2}. This difference mainly arises due to the lesser availability of the solar radiation in the month of January compared to November. It can also be noticed that the SWDOWN is more sensitive to the changes in the optical properties of the carbonaceous aerosols compared to the mineral dust species. The mean changes in SWDOWN due to the modification in the optical properties of mineral dust (EXP2) is +1.4 and -0.73 W m^{-2} during Event-I and Event-II respectively (Table S6). On the other hand, those due to the changes in the optical properties of BC (EXP3) and OC (EXP4) are -22.46, -9.34; and -11.35, -5.69 W m^{-2} during Event-I and Event-II respectively. It may be noted that the real parts (scattering ability) of the RIs of aerosol have not been substantially modified in this study (Table 1). The major modifications have occurred in the imaginary parts (absorption ability). Moreover, the changes in the imaginary parts of BC and OC are much higher in magnitude than that in the imaginary parts of the RI of dust. Therefore, EXP3 (BC) and EXP4 (OC) produce more changes in SWDOWN compared to the EXP2 (Dust). The mean changes in SWDOWN during clear-sky due to EXP5 (All-Species) are -27.52 W m^{-2} and -13.39 W m^{-2} for the Event-I and Event-II respectively. With the noon-time values going as high as 50 W m^{-2} and 25 W m^{-2} respectively, which are roughly (⅓)rd to (¼)th of the total impacts of direct radiative effects of aerosols.

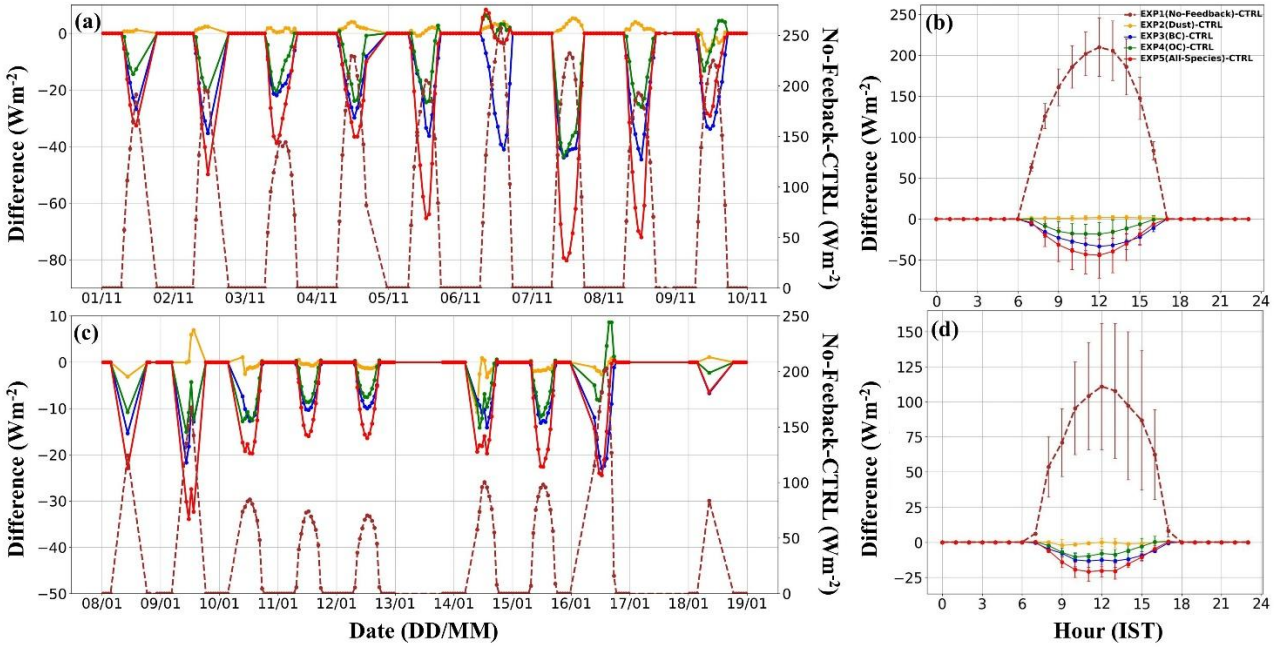

https://doi.org/10.5194/egusphere-2026-1100
Preprint. Discussion started: 24 March 2026

Fig. 4. Reduction in simulated SWDOWN in EXP2, EXP3, EXP4, and EXP5 configurations with respect to CTRL along with difference of EXP1 configuration and CTRL during (a) Event-I, and (c) Event-II in clear-sky. Diurnal changes in simulated averaged SWDOWN during (b) Event-I, and (d) Event-II in clear-sky.

The changes in SWDOWN due to changes in the optical properties of all aerosol species are around 20 % (in magnitude) less than the sum of the changes in SWDOWN due to the modification of individual species' optical properties, suggesting that the changes in SWDOWN are not strictly linear and additive.

3.3 Effects of the modified aerosol optical properties on meteorological parameters

We now examine the impacts of modified optical properties of aerosols on the meteorological parameters mainly through the direct radiative interaction and the fast-atmospheric response to those. We compare the impacts on the near-surface temperatures (T2), relative humidity (RH2) levels, wind speeds (WS10), and the simulated planetary boundary layer height (PBLH). We compare the simulated values with the corresponding measurements carried out at the WiFEX measurement site at the IGI Airport, New Delhi in Fig. 5. Figures 5a, 5c, 5e, and 5g, depict the comparisons between the meteorological parameters simulated by CTRL and EXP5 (All-Species) configurations, and the measurements, for the Event-I. Figures 5b, 5d, 5f, and 5h, shows the impacts of modified optical properties of aerosols on the simulated meteorological parameters in the model. For T2, it may be seen that both the model configurations underestimate the temperatures during the pre-noon hours and overestimate those in the afternoon through early midnight hours. The modifications in the optical properties results in the reduction of surface temperatures by 0.2 °C in the morning hours, while the post-noon enhancements in temperatures also reach up to 0.3 °C. The early morning reduction in the temperatures is expected as the more optically thick aerosol mixture in the EXP5 (All-Species) configuration scatters and absorbs more incoming shortwave radiation than that in the CTRL configuration thus resulting in surface-cooling. As a consequence, the RH2 values are also seen to be higher in the EXP5 (All-Species) configuration vis-a-vis CTRL case. On an average the changes in RH2 are ~2-4 %. Nevertheless, the simulated RH2 values are much lesser compared to the measurements. One of the reasons behind this underestimation in RH could be related to the drier soil moisture levels in the model, as shown by Parde et al., 2022. The changes in WS10 due to the modified optical properties of aerosols are however relatively higher and sustained morning through evening. On an average, the winds are found to be calmer in the EXP5 (All-Species) configuration vis-a-vis CTRL. The maximum reductions of around 0.4 m s^{-1} are seen to be during the 12–16 LT with the mean winds in the CTRL configuration around 2.5–3.25 m s^{-1}. Thus, the near-surface winds are seen to be slowing down by ~12-16 %, throughout the day, with maximum changes during the afternoon hours. This in turn also results in better agreements with the observations in comparison with the CTRL run.

https://doi.org/10.5194/egusphere-2026-1100
Preprint. Discussion started: 24 March 2026

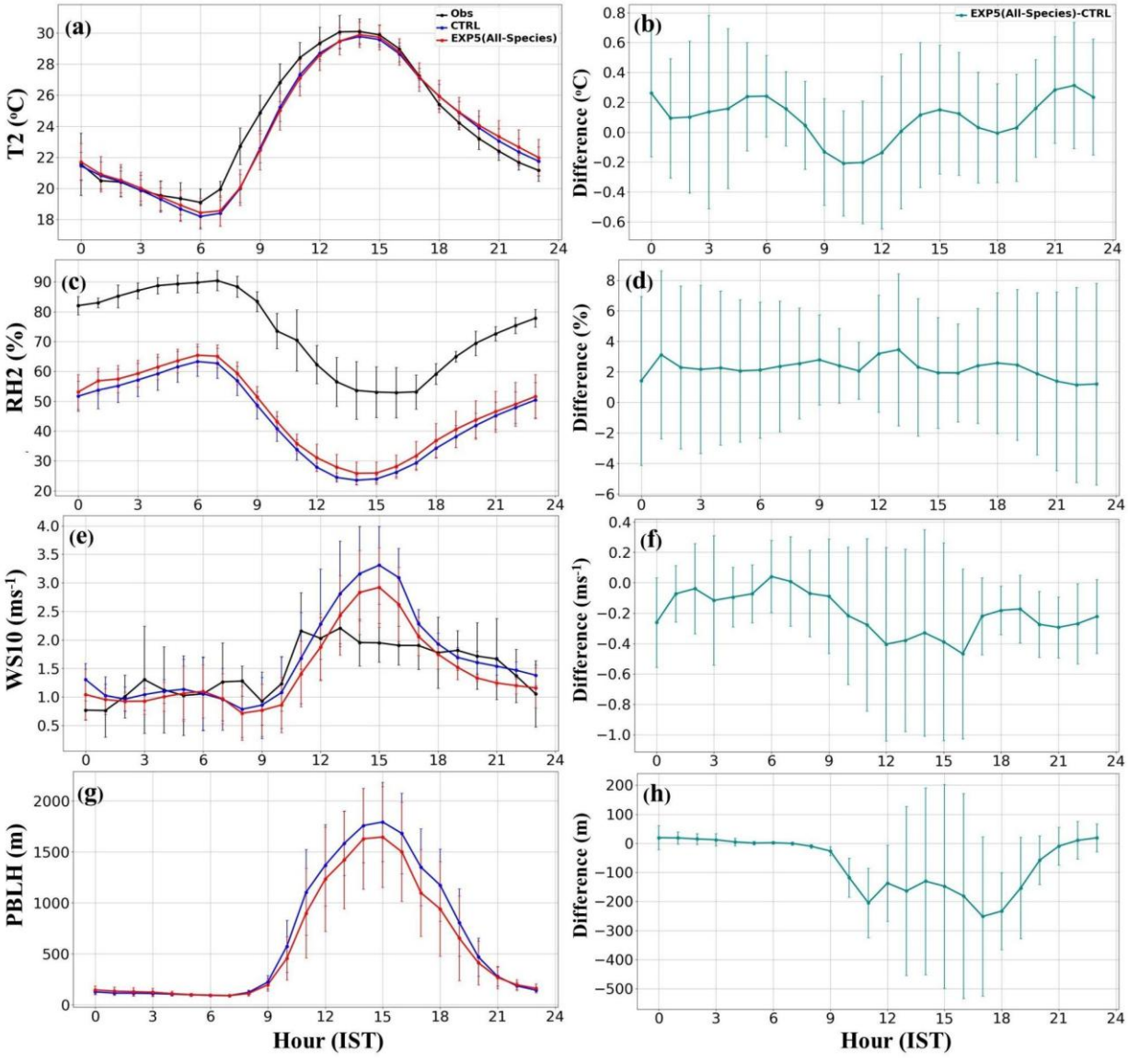

Fig. 5: Diurnal cycle of simulated meteorological parameters in CTRL and EXP5 along with observations, and changes in EXP5 with respect to CTRL for Event-I under clear-sky: (a) and (b) for T2, (c) and (d) for RH2, (e) and (f) for WS10, and (g) and (h) for PBLH.

The MB, RMSE, NMSE, and the FB are 0.20 (0.01) m s^{-1}, 0.83 (0.75) m s^{-1}, 0.283 (0.262), and 0.115 (-0.01) for the CTRL (EXP5) experiment (Table S4). As a result of reduction in surface temperature and near-surface wind speeds, the boundary layer turbulence is also expected to be reduced in EXP5 (All-Species) configuration. The PBLH which represents the level of turbulence in the planetary boundary layer is seen to be reduced in the EXP5 (All-Species) configuration vis-a-vis CTRL.

https://doi.org/10.5194/egusphere-2026-1100
Preprint. Discussion started: 24 March 2026

The mean reductions are seen to be as high as 200-300 m during the afternoon hours, which are ~15-20 % of PBLH in CTRL configuration. Thus, changes in optical properties also reduce the turbulence in the lower atmosphere, which could result in lesser mixing of near-surface aerosols across the atmospheric column.

Similar analysis of the impacts of the modified optical properties of aerosols on the meteorological parameters has been performed for the Event-II of extreme pollution. The results are shown in supplementary Fig. S4**.** Similar to the Event-I, the modification of aerosol optical properties results in colder near-surface temperatures (change of -0.2 °C in T2) for the Event-II too. The consequent enhancements (of 1-2 %) in RH are also noticed. Similarly, the wind speeds also seem to reduce by around 0.2 m s^{-1} in the modified configuration. The PBLH also shows a decline by 40-50 m in EXP5 (All-Species) configuration vis-a-vis CTRL. It may be noticed that the changes in all the analysed meteorological parameters in the month of January are lesser compared to that in the month of November. As mentioned previously, this behaviour is primarily due to the lesser availability of solar radiation in the month of January, which reduces the magnitude of the impact that modified aerosols have on the radiation and thus limits the atmospheric response to the perturbations. Nevertheless, the nature and the sign of the impacts on meteorological parameters remains similar to that in November.

The reduced winds speeds and boundary layer heights would result in reduced ventilation coefficient (VC) in the EXP5 (All-Species) configuration vis-a-vis CTRL. The same has been verified in Fig. 6. The VC which is the product of PBLH and winds in the PBL, has been plotted for both the events, for CTRL as well as EXP5 (All-Species) configuration (Figs. 6a and 6c). The changes in VC have also been plotted in Figs. 6b and 6d.

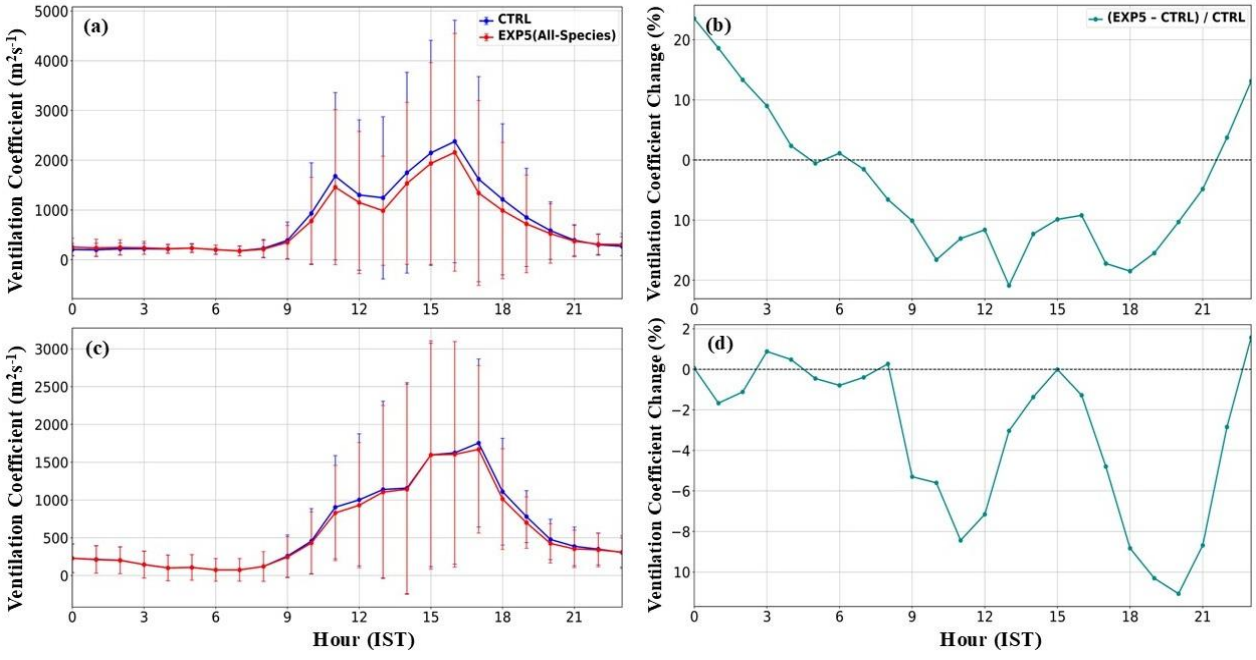

https://doi.org/10.5194/egusphere-2026-1100
Preprint. Discussion started: 24 March 2026

Fig. 6. Diurnal cycle of ventilation coefficient in CTRL and EXP5, and percentage change in EXP5 with respect to CTRL (right): (a) and (b) for Event-I, and (c) and (d) for Event-II under clear-sky.

It may be noted that the VC maximizes during the afternoon hours mainly due to higher boundary layer heights owing to the well-mixed boundary layer. Conversely, the lowest values of VC are noticed during the evening to early morning hours (Figs. 6a and 6c) due to shallow boundary layer and calmer winds. It may be noted that the VC in the 'EXP5 (All-Species)' is consistently lower compared to that in the CTRL configuration, especially during the sunlit hours and even after sunset. The mean reductions are up to 20 % in the month of November (Event-I), and up to 10-12 % in the month of January (Event-II). The maximum changes are expectedly seen during the sunlit hours, while they are less in magnitude and/or in relative terms during the night hours.

3.4. Effects of the modified aerosol optical properties on the near-surface $PM_{2.5}$ mass concentrations

The VC governs the near-surface concentration of aerosols (Govardhan et al., 2015). The higher (lower) values VC signifies greater (reduced) horizontal advection and vertical mixing aerosols in the atmosphere. As shown in Fig. 6, VC in the EXP5 (All-Species) configuration is reduced throughout the sunlit hours of the day, one would expect a consequent increase in the near-surface mass concentrations of $PM_{2.5}$ in the model. To confirm that, we have examined the near-surface mass concentrations of $PM_{2.5}$ in both the configurations and for both the events in Fig. 7.

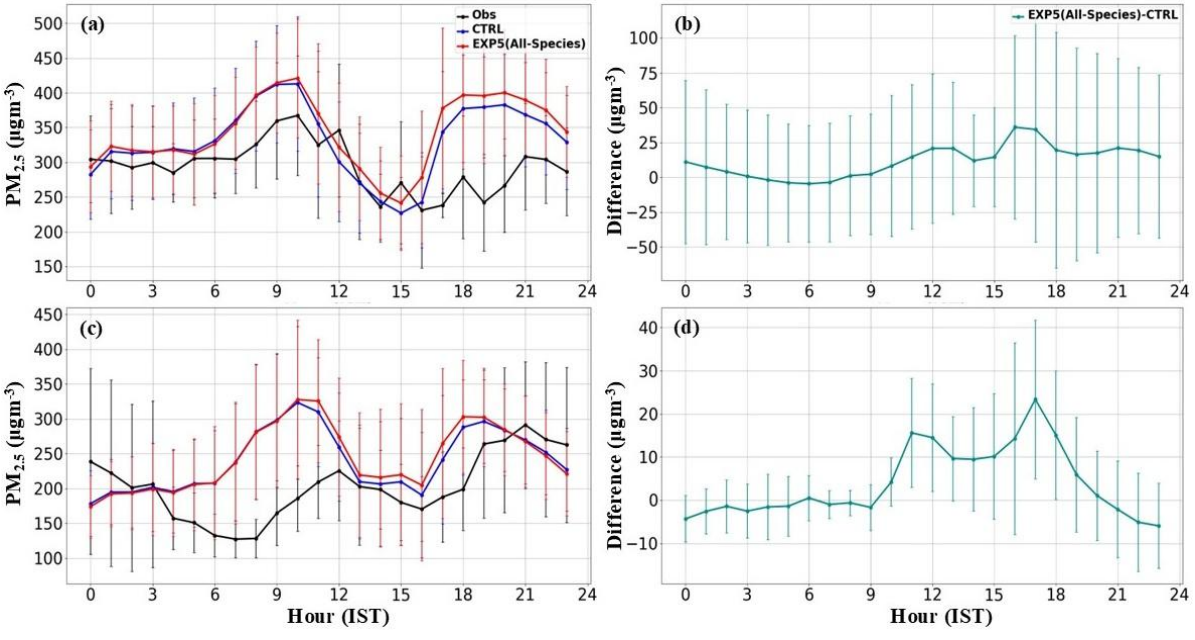

https://doi.org/10.5194/egusphere-2026-1100
Preprint. Discussion started: 24 March 2026

Fig. 7. Diurnal cycle of averaged simulated $PM_{2.5}$ mass concentrations in CTRL and EXP5 along with observations and changes in EXP5 with respect to CTRL: (a) and (b) for Event-I, and (c) and (d) for Event-II under clear-sky.

It may be seen that the $PM_{2.5}$ indeed increases EXP5 (All-Species) configuration vis-a-vis CTRL. The mean changes are seen to be the highest during the afternoon hours. On average, the maximum changes during the polluted events are ~37-40 µg m^{-3} for the November-event (I) and ~25 µg m^{-3} during the January-event (II). For the Event-I, the mass concentrations show enhancements throughout the day barring minor reductions during some late-night to early morning hours. On the other hand, for the Event-II, the increments in $PM_{2.5}$ are seen only during the period of 10:00 to 20:00 LT. Nevertheless, during the sunlit hours the mass concentrations of $PM_{2.5}$ show expected enhancements.

The overall impacts of modifications in the optical properties of aerosols are depicted in Fig. 8. The modified more absorbing aerosol species reduce the downwelling shortwave radiation reaching the surface, thus reducing the surface temperature, near-surface winds, and turbulence in the planetary boundary layer. The resulting reduced PBLH and wind speeds limit the ventilation of aerosols in the atmosphere. This further enhances the surface-level concentrations of aerosols thus leading to even further extinction of the incoming solar radiation, hence giving positive feedback to the entire loop.

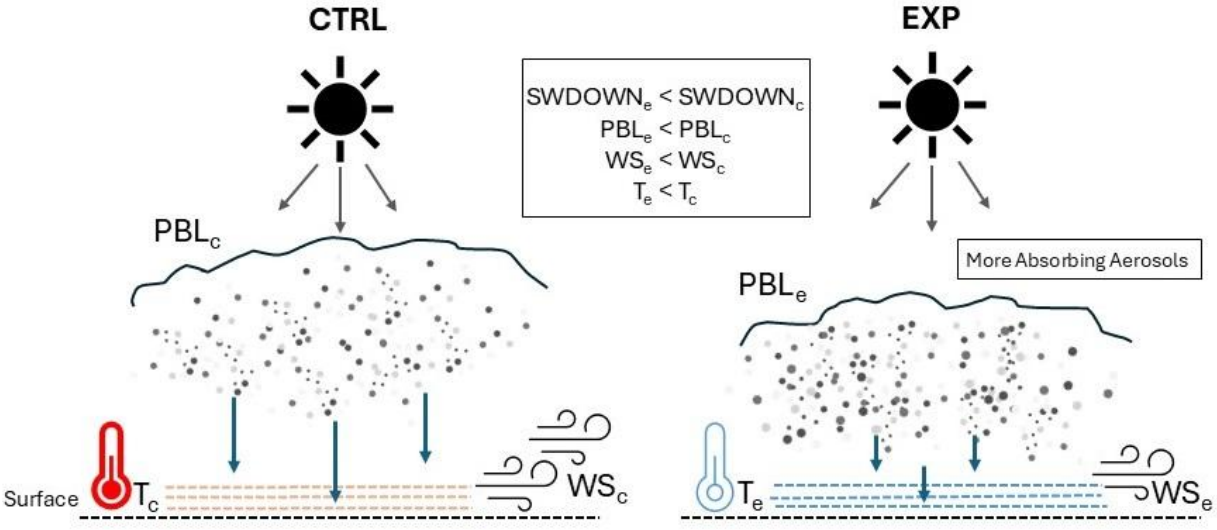

Fig. 8. Schematic of physical processes mechanism involved in CTRL and EXP (All-Species) configurations. Here, c denotes CTRL and e denotes EXP5.

https://doi.org/10.5194/egusphere-2026-1100
Preprint. Discussion started: 24 March 2026

3.5 Effects of modified optical properties of aerosol: monthly-mean picture

To examine the effects of the modifications in the optical properties of aerosols on meteorological as well as aerosol related parameters on a longer timescale, we carried out four month-long simulations (for domain d01 and d02) of WRF-Chem for the months of October, November, December of 2023 and January 2024, in CTRL, and all other sensitivity configurations. The clear-sky impacts of modifications in optical properties of individual aerosol species and that of the all species put together on the surface reaching downwelling shortwave radiation from domain d01 is shown in Fig. 9 and from d02 in Fig. S5. Similar to that for the extreme pollution events, the impacts of modified optical properties of dust aerosols alone have minimal effect on SWDOWN. This is partly due to the fact that the period under consideration in this study is mainly post-monsoon and winter, which has relatively slower winds and humid conditions, thus lesser long-range transport of mineral dust from the deserts of Thar and Arabia to Delhi. This limits the concentrations of mineral dust over this region vis-a-vis the pre-monsoonal months of March to May. Moreover, as discussed in Table 2, even after modification the imaginary part of the RIs of dust is still much lesser than that for BC or OC, hence the consequent impacts of the modification in mineral dust RI as minimal.

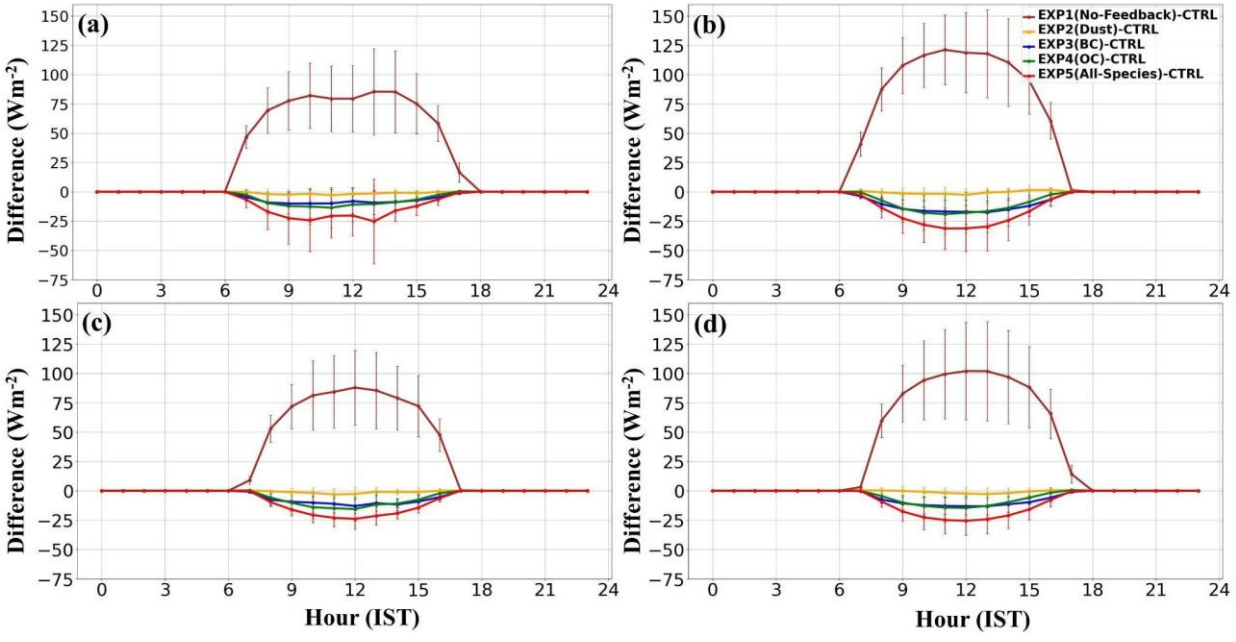

Fig. 9. Diurnal cycle of changes in averaged SWDOWN for EXP1, EXP2, EXP3, EXP4, and EXP5 with respect to CTRL in d01 simulations under clear-sky over Delhi: (a) October 2023, (b) November 2023, (c) December 2023, and (d) January 2024.

https://doi.org/10.5194/egusphere-2026-1100
Preprint. Discussion started: 24 March 2026

The SWDOWN reduces by as high as ~12 W m^{-2} at the noon time, across all the months barring November, due to the changes in the RI of OC and BC individually. For November, the corresponding changes are twice (~25 W m^{-2}) of that for the other months. This is mainly due to the enhanced concentrations of these aerosol species in November mainly owing to the agricultural burning activities that occur predominantly in the neighbouring states of Punjab and Haryana in north-western India. The maximum impacts of the modifications in RIs of all aerosols crosses 25 (37) W m^{-2} for October, December, and January (November). As shown previously also, the noontime impacts of ARI on the SWDOWN at surface go as high as 80-100 W m^{-2} for October, December, and January, while that for November goes beyond 120 W m^{-2}. Therefore, as shown for the pollution episodes, the impacts of modifications in the RIs of aerosols are around (⅓)rd to (¼)th of the total impacts of aerosols on radiation in WRF-Chem, even on monthly-mean timescales. Thus, the modifications induce substantial changes in the total ARI in WRF-Chem over this region. It is noteworthy that results from the coarser domain (d01; 10 km resolution) do not differ significantly from those of the finer domain (d02; 2 km resolution). A detailed comparison of simulated SWDOWN for CTRL and EXP1 to EXP5 across all months under clear-sky conditions is provided in the supplement (Tables S7 and S8).

Comparison with WiFEX observed shortwave fluxes for December 2023 and January 2024 further demonstrates improvement in model performance. Under clear-sky (non-foggy) conditions, the mean SWDOWN bias is substantially reduced in the EXP5 (All-Species) configuration relative to CTRL (Table S9). In December, the mean bias decreased from 10.53 W m^{-2} in CTRL to 3.96 W m^{-2} in EXP5 (~62 % reduction). In January, it decreased from 23.63 W m^{-2} to 15.26 W m^{-2} (~35 % reduction). These reductions demonstrate that improved representation of ARI through revised aerosol optical properties enhances model skill. Incorporating more realistic aerosol optical parameters in operational air quality forecasting systems can therefore strengthen aerosol–meteorology feedback representation and improve pollution predictability.

The associated impacts of the modified RIs of aerosols on the meteorological parameters as well as $PM_{2.5}$ concentrations on the monthly-mean time scales are tabulated in Table 3. As shown in Fig. 9, the monthly-mean SWDOWN in EXP5 configuration is lesser than the CTRL configuration for all the months by around 16-20 W m^{-2}. The numbers are expectedly smaller than the noon-time maximums shown in Fig. 11. The resultant changes in T2 are also evident especially for the months of December and January, albeit with subdued values. The mean RH2 in the model shows greater changes (5-10 %) in the months of December and January, while showing changes of ~2-3 % in October and November. The near-surface wind speeds (WS10) show a reduction on a monthly-mean basis. Similarly, the monthly-mean PBLH depicts a reduction across all the months upon modification in the RIs. The consequent changes in the monthly-mean near-surface $PM_{2.5}$ mass concentrations are also evident, though smaller in magnitudes, being on monthly-mean scale, they still convey the same message that Fig. 8 and the analysis prior to that so.

Table 3. Monthly averaged changes in meteorological variables (SWDOWN, T2, RH2, WS10, PBLH) and $PM_{2.5}$ mass concentrations from October 2023 to January 2024 in d01 simulations under clear sky over Delhi.

https://doi.org/10.5194/egusphere-2026-1100
Preprint. Discussion started: 24 March 2026

Month	October 2023		November 2023		December 2023		January 2024	
	CTRL	EXP5	CTRL	EXP5	CTRL	EXP5	CTRL	EXP5
SWDOWN ($W\ m^{-2}$)	461.15	445.23	376.58	356.50	368.18	352.61	358.52	342.82
T2 (°C)	31.55	31.72	25.81	25.99	19.71	19.42	19.29	18.85
RH2 (%)	36.03	38.05	40.60	42.27	44.42	48.04	37.18	47.40
WS10 ($m\ s^{-1}$)	3.78	3.76	1.89	1.85	2.45	2.37	2.63	2.62
PBLH (m)	1058.23	1047.27	835.16	809.50	619.95	565.10	776.12	688.45
$PM_{2.5}$ ($\mu g\ m^{-3}$)	128.68	127.02	207.87	213.41	169.10	173.95	188.94	192.64

4 Discussion

Thus, the revised optical properties of aerosols in WRF-Chem result in optically thicker and more absorbing aerosols. They in-turn reduce the downwelling shortwave radiation reaching the surface, thus showing better agreements with the corresponding observations. The resultant changes in near-surface temperatures, winds and boundary layer heights enhance the surface concentrations of simulated $PM_{2.5}$, especially during the daytime. These enhancements are particularly important for the AIRWISE system, as the system-simulated $PM_{2.5}$ shows a rapid decline during the sunlit hours, and misses the morning-time concentrations (Ghude et al., 2024; Sengupta et al., 2022). The model seems to over-ventilate the pollutants. In fact, AIRWISE better captures the night-time peaks in $PM_{2.5}$ concentrations, however mainly due to its inability in capturing the morning time concentrations, the simulated Air Quality Index (AQI), which is calculated on the basis of 24-hour-running-mean values of $PM_{2.5}$, shows mis-match vis-a-vis observed AQIs. Therefore, the modifications in the optical properties are expected to improve the performance of the AIRWISE system in capturing the AQI and provide improved warnings to the policymakers about forthcoming air pollution episodes.

As noticed in Fig. 3, the bias in the simulated SWDOWN vis-a-vis the observations still exist. One of the major parameters that can reduce the bias would be the urban morphology. The WRF-Chem model employed in this study and that used in the AIRWISE system does not include urban morphology in its formulation. The urban structures reflect and absorb the direct as well as diffused sunlight and thus reduce SWDOWN reaching the surface. Therefore, lack of urban structures in

https://doi.org/10.5194/egusphere-2026-1100
Preprint. Discussion started: 24 March 2026

the model may have resulted in the overestimation of SWDOWN at the surface. The simulated surface temperatures still are biased vis-a-vis the observations. In addition to the urban morphology, this behaviour of the model may also be linked with the soil moisture levels. It has been shown previously that WRF tends to have biases in the simulated soil moisture in northern-India especially in post-monsoon to winter months (Parde et al., 2022). The latest land-use land category data along with the correct information about the extent of irrigation in the fields may improve the simulated soil-moisture and thus the near-surface temperatures in the model. One of the other limitations of this study is related to the lack of observational data for the solar radiation measurements. Currently, the data available over the WiFEX observational site has been used; however, more such data locations are needed to validate our findings. Unfortunately, due to lack of systematic in dataset for radiative fluxes especially over the NCR, the study had to be limited to only one observational location. In future, it is recommended that a network of sites with radiation measurements needs to be established to further strengthen the model.

It has been shown that even after modifying the optical properties of aerosols, the model still shows biases for the simulated near-surface $PM_{2.5}$ mass concentrations. It may be noted that the emission inventory used in this study as well as in the AIRWISE system is old and it needs update keeping in mind the technological as well as administrative changes that have occurred over the study domain in the last few years. Moreover, instead of having a static emissions inventory, it will be useful to employ the dynamic emissions inventory in the model which dynamically estimates the emissions based on real-time capture of vehicular traffic, construction and demolition activities, waste burning and other related activities. As noticed in our analysis, one of the major uncertainties in the aspect of emissions of particulate pollutants exists in the agricultural burning related emissions. The exact timing of the farm fires, the locations, the amount of the crop residue being burnt, and subsequent emissions of pollutants generated from the farm fires contribute to the overall uncertainty in the estimates as discussed by Ambulkar et al., 2025. It has also been shown by Ghude et al., 2024 that the system mainly shows less skill in the month of November when the farm fires are at their peak, thus underscoring their impact on the simulations. The use of burnt area indices from a very high-resolution satellite-data base like Sentinel-2, instead of fire count information may assist in better capture of the fire locations. Further, the chemical mechanism used in the WRF-Chem model for AIRWISE purposes, is rather simple and lacks comprehensive treatment to secondary organic aerosols or some of the secondary inorganic aerosols (like nitrates) too. In future, fast chemical parameterization for the inclusion of these species may be exercised. Additionally, to improve the performance of the model in simulating the composition of $PM_{2.5}$, more measurements of the chemical composition may be carried out in areas of heavy pollution.

5 Conclusion

Air pollution remains one of the most critical environmental challenges over northern India, particularly during the post-monsoon and winter seasons when stagnant meteorological conditions, biomass burning, and enhanced aerosol loading frequently lead to severe pollution episodes. Accurate forecasting of such extreme air quality events is essential for

https://doi.org/10.5194/egusphere-2026-1100
Preprint. Discussion started: 24 March 2026

policymakers and public health authorities to mitigate population exposure and implement timely emission-control strategies.

The Air Quality Warning and Integrated Decision Support System for Emissions (AIRWISE), developed through a collaborative effort between the Indian Institute of Tropical Meteorology (IITM), the India Meteorological Department (IMD), and the National Center for Atmospheric Research (NCAR), has been operational since 2018 and provides real-time air quality forecasts across India. Despite its operational success, the system exhibits limitations in reproducing extreme pollution loading events over northern India, particularly over Delhi during the crop-residue (stubble) burning season in the surrounding states. These high-impact episodes are often underestimated partly due to inaccuracies in representing aerosol–radiation–meteorology interactions. Improving the representation of meteorological feedback processes is therefore crucial for enhancing forecast skill. Among these processes, shortwave radiation plays a pivotal role in governing boundary layer evolution, surface energy balance, atmospheric stability, and pollutant dispersion. In many numerical weather and chemistry models, aerosol optical properties are prescribed using globally averaged values, which may not adequately represent the complex and highly absorbing aerosol mixtures characteristic of northern India. Such simplifications introduce biases in surface radiation fluxes, subsequently affecting boundary layer dynamics and pollutant accumulation.

This study demonstrates that incorporating region-specific aerosol optical properties, such as observed refractive indices of dominant chemical species, significantly improves the simulation of surface shortwave radiation, reducing flux biases by 25-37 W m^{-2} on monthly scales and by up to ~80 W m^{-2} during severe polluted episodes. The revised aerosol–radiation interaction modifies the surface energy budget, decreasing surface temperature (~0.2 °C), near-surface wind speed (~0.4 m s^{-1}), and planetary boundary layer height (~200 m), while increasing daytime relative humidity by 3–4 % under polluted conditions ($PM_{2.5}$ > 400–550 µg m^{-3}), thereby enhancing the model's ability to reproduce high surface pollutant concentrations (20-40 µg m^{-3}) during extreme events. These improvements highlight the importance of using locally constrained aerosol optical parameters rather than relying on global averages in regions with complex aerosol compositions.

However, to extend and generalize these findings across the broader Indian region, additional surface radiation measurements are required. Expanded observational coverage would enable more robust model validation, reduce uncertainties in aerosol optical parameterization, and further enhance the predictive capability of operational air quality forecasting systems such as AIRWISE.

Appendix A

Acronym	Description
AF	Asymmetric Factor

https://doi.org/10.5194/egusphere-2026-1100
Preprint. Discussion started: 24 March 2026

AIRWISE	Air Quality Warning and Integrated Decision Support System for Emissions
AOD	Aerosol Optical Depth
ARI	Aerosol-Radiation Interaction
AQI	Air Quality Index
AWS	Automated Weather Stations
BC	Black Carbon
CAM	Community Atmosphere Model
CRTM	Community Radiative Transfer Model
CPCB	Central Pollution Control Board
CTRL	Control Run
d01	Outer Domain
d02	Inner Domain
DPCC	Delhi Pollution Control Committee
EC	Elemental Carbon
ECMWF	European Centre for Medium-Range Weather Forecast
EDGAR-HTAP	Emission Database for Global Atmospheric Hemispheric Transport of Air Pollution
ERA5	ECMWF Fifth Generation Reanalysis
EXP1(No-Feedback)	Experiment with No Aerosol-Radiation Feedback
EXP2(Dust)	Experiment with Modified Refractive Index of Dust only
EXP3(BC)	Experiment with Modified Refractive Index of BC only
EXP4(OC)	Experiment with Modified Refractive Index of OC only
EXP5(All-Species)	Experiment with Modified Refractive Index of Dust, BC, OC, and P25
FB	Fractional Bias
FINN	Fire Inventory from NCAR
GOCART	Goddard Chemistry Aerosol Radiation and Transport
IGBP	International Geosphere-Biosphere Programme

https://doi.org/10.5194/egusphere-2026-1100
Preprint. Discussion started: 24 March 2026

IGI	Indira Gandhi International
IGP	Indo Gangetic Plains
IITM	Indian Institute of Tropical Meteorology
IMD	India Meteorological Department
IST	Indian Standard Time
LAC	Light Absorbing Carbon
LT	Local Time
MB	Mean Bias
MEGAN	Model for Emissions of Gases and Aerosol from Nature
MODIS	Moderate Resolution Imaging Spectroradiometer
MOZART	Model for Ozone and Related Tracers
MYNN	Mellor-Yamada Nakanishi and Niino
NCAR	National Center for Atmospheric Research
NCR	National Capital Region
NMSE	Normalized Mean Square Error
NWP	Numerical Weather Prediction
OC	Organic Carbon
P25	Other GOCART Primary $PM_{2.5}$
PBLH	Planetary Boundary Layer Height
$PM_{2.5}$	Particulate Matter of Diameter 2.5 µm or less
PM_{10}	Particulate Matter of Diameter 10 µm or less
RH2	Relative Humidity at 2 m
RI	Refractive Index
RMSE	Root Mean Square Error
RRTMG	Rapid Radiative Transfer Model for Global
SSA	Single Scattering Albedo
SWDOWN	Downward Shortwave Radiation

https://doi.org/10.5194/egusphere-2026-1100
Preprint. Discussion started: 24 March 2026

T2	Temperature at 2 m
WiFEX	Winter Fog Experiment
WRF	Weather Research and Forecasting
WRF-Chem	WRF coupled with Chemistry
WS10	Wind Speed at 10 m
WM6	WRF Single-Moment 6-class

Code and data availability

Code and data availability

The WRF-Chem model source code is publicly available from the National Center for Atmospheric Research (NCAR) at https://www2.mmm.ucar.edu/wrf/users/download/get_source.html. WiFEX 2023–24 observational datasets are available at https://ews.tropmet.res.in/wifex/index.php. Surface $PM_{2.5}$ observations were obtained from the Central Pollution Control Board (CPCB) Central Control Room portal (https://app.cpcbccr.com/ccr/, currently redirected to https://aqinow.org/ccr). The WRF-Chem model configuration files, modified module codes, simulations output and analysis scripts generated in this study are available from the corresponding author upon reasonable request. Data processing and visualization were performed using Python (https://www.python.org/) with standard scientific libraries and OriginPro (OriginLab Corporation, https://www.originlab.com/).

Author contributions

Sumit Kumar: Conceptualization, Methodology, Simulations, Model development, Software, Formal analysis, Investigation, Data curation, Visualization, Writing – original draft, Writing – review and editing.

Gaurav Govardhan: Conceptualization, Methodology, Model development, Supervision, Visualization, Writing – review and editing.

Sreyashi Debnath: Simulations, Methodology, Formal analysis, Validation.

Avinash N. Parde: Methodology, Simulations, Writing – review and editing.

Sandeep Wagh: Data curation, Technical support.

Jimy Dudhia: Model development, Software, Writing – review.

Sachin D. Ghude: Conceptualization, Supervision, Funding acquisition, Project administration, Writing – review and editing.

https://doi.org/10.5194/egusphere-2026-1100
Preprint. Discussion started: 24 March 2026

Competing interests

The authors have no relevant financial or non-financial interests or conflict to disclose.

Acknowledgements

The authors sincerely acknowledge the Central Pollution Control Board (CPCB) and the Delhi Pollution Control Committee (DPCC) for providing the $PM_{2.5}$ measurement data used for model evaluation. The numerical simulations were performed on the *Pratyush* supercomputing facility at the Indian Institute of Tropical Meteorology (IITM), Pune. We gratefully acknowledge the Director, IITM; the Director-General, India Meteorological Department (IMD), New Delhi; and the Head, National Centre for Medium-Range Weather Forecasting (NCMRWF), Noida, for their continued encouragement and institutional support, particularly during the Winter Fog Experiment (WiFEX) campaign. The Ministry of Earth Sciences (MoES), Government of India, is also acknowledged for sustained support of the campaign activities. We thank the Grandhi Mallikarjuna Rao (GMR) Group and the Airports Authority of India (AAI) for logistical support at Indira Gandhi International (IGI) Airport, New Delhi. Finally, we appreciate the handling editor and the anonymous reviewers for their constructive comments, which significantly improved the manuscript.

References

Adler, G., Riziq, A. A., Erlick, C., and Rudich, Y. (2010). Effect of intrinsic organic carbon on the optical properties of fresh diesel soot. Proceedings of the National Academy of Sciences, 107(15), 6699-6704.

Agnihotri, R., Mishra, S. K., Yadav, P., Singh, S., Rashmi, Prasad, M. V. S. N., ... and Arya, B. C. (2015). Bulk level to individual particle level chemical composition of atmospheric dust aerosols (PM5) over a semi-arid urban zone of Western India (Rajasthan). Aerosol and air quality research, 15(1), 58-71.

Ambulkar, R., Govardhan, G., Gavhale, S., Kalita, G., Pande, C., Jat, R., ... and Ghude, S. D. (2025). Crop residue burning in north-western India: Emission estimation and uncertainty quantification. Journal of Geophysical Research: Atmospheres, 130(4), e2024JD042198.

Baklanov, A., Schlünzen, K., Suppan, P., Baldasano, J., Brunner, D., Aksoyoglu, S., ... and Zhang, Y. (2014). Online coupled regional meteorology chemistry models in Europe: current status and prospects. Atmospheric Chemistry and Physics, 14(1), 317-398.

Barnard, J. C., Fast, J. D., Paredes-Miranda, G., Arnott, W. P., and Laskin, A. (2010). Evaluation of the WRF-Chem" Aerosol Chemical to Aerosol Optical Properties" Module using data from the MILAGRO campaign. Atmospheric Chemistry and Physics, 10(15), 7325-7340.

Bellouin, N., Quaas, J., Gryspeerdt, E., Kinne, S., Stier, P., Watson-Parris, D., ... and Stevens, B. (2020). Bounding global aerosol radiative forcing of climate change. Reviews of Geophysics, 58(1), e2019RG000660.

https://doi.org/10.5194/egusphere-2026-1100
Preprint. Discussion started: 24 March 2026

Bender, F. A. M. (2020). Aerosol forcing: Still uncertain, still relevant. AGU advances, 1(3), e2019AV000128.

Bond, T. C., and Bergstrom, R. W. (2006). Light absorption by carbonaceous particles: An investigative review. Aerosol science and technology, 40(1), 27-67.

Businger, J. A., Wyngaard, J. C., Izumi, Y., and Bradley, E. F. (1971). Flux-profile relationships in the atmospheric surface layer. Journal of Atmospheric Sciences, 28(2), 181-189.

Chang, H. C., and Charalampopoulos, T. T. (1990). Determination of the wavelength dependence of refractive indices of flame soot. Proceedings of the Royal Society of London. Series A: Mathematical and Physical Sciences, 430(1880), 577-591.

Chen, F., and Dudhia, J. (2001). Coupling an advanced land surface–hydrology model with the Penn State–NCAR MM5 modeling system. Part I: Model implementation and sensitivity. Monthly weather review, 129(4), 569-585.

Chen, Y., and Bond, T. C. (2010). Light absorption by organic carbon from wood combustion. Atmospheric Chemistry and Physics, 10(4), 1773-1787.

Chin, M., Rood, R. B., Lin, S. J., Müller, J. F., and Thompson, A. M. (2000). Atmospheric sulfur cycle simulated in the global model GOCART: Model description and global properties. Journal of Geophysical Research: Atmospheres, 105(D20), 24671-24687.

Chou, M. D., and Suarez, M. J. (1999). A solar radiation parameterization for atmospheric studies (No. NASA/TM-1999-104606/VOL15).

Collins, W. D., Rasch, P. J., Boville, B. A., Hack, J. J., McCaa, J. R., Williamson, D. L., ... and Dai, Y. (2004). Description of the NCAR community atmosphere model (CAM 3.0). NCAR Tech. Note NCAR/TN-464+ STR, 226, 1326-1334.

Emmons, L. K., Walters, S., Hess, P. G., Lamarque, J. F., Pfister, G. G., and Tie, X. X. (2010). Description and evaluation of the Model for Ozone and Related chemical Tracers, version 4 (MOZART-4). Geoscientific Model Development, 3(1), 43-67. https://doi.org/10.5194/gmd-3-43-2010

Fast, J. D., Gustafson Jr, W. I., Easter, R. C., Zaveri, R. A., Barnard, J. C., Chapman, E. G., ... and Peckham, S. E. (2006). Evolution of ozone, particulates, and aerosol direct radiative forcing in the vicinity of Houston using a fully coupled meteorology-chemistry-aerosol model. Journal of Geophysical Research: Atmospheres, 111(D21).

Friedl, M. A., McIver, D. K., Hodges, J. C., Zhang, X. Y., Muchoney, D., Strahler, A. H., ... and Schaaf, C. (2002). Global land cover mapping from MODIS: algorithms and early results. Remote sensing of Environment, 83(1-2), 287-302.

Ghan, S., Laulainen, N., Easter, R., Wagener, R., Nemesure, S., Chapman, E., ... and Leung, R. (2001). Evaluation of aerosol direct radiative forcing in MIRAGE. Journal of Geophysical Research: Atmospheres, 106(D6), 5295-5316.

Ghude, S. D., Bhat, G. S., Prabhakaran, T., Jenamani, R. K., Chate, D. M., Safai, P. D., ... and Rajeevan, M. (2017). Winter fog experiment over the Indo-Gangetic plains of India. Current Science, 767-784.

Ghude, S. D., Kumar, R., Jena, C., Debnath, S., Kulkarni, R. G., Alessandrini, S., ... and Rajeevan, M. (2020). Evaluation of PM 2.5 forecast using chemical data assimilation in the WRF-Chem model. Current Science, 118(11), 1803-1815.

https://doi.org/10.5194/egusphere-2026-1100
Preprint. Discussion started: 24 March 2026

Ghude, S. D., Jenamani, R. K., Kulkarni, R., Wagh, S., Dhangar, N. G., Parde, A. N., ... and Rajeevan, M. (2023). WiFEX: walk into the warm fog over Indo-Gangetic Plain region. Bulletin of the American Meteorological Society, 104(5), E980-E1005.

Ghude, S. D., Govardhan, G., Kumar, R., Yadav, P. P., Jat, R., Debnath, S., ... and Rajeevan, M. (2024). Air quality warning and integrated decision support system for emissions (AIRWISE): Enhancing air quality management in megacities. Bulletin of the American Meteorological Society, 105(12), E2525-E2550.

Glotfelty, T., Alapaty, K., He, J., Hawbecker, P., Song, X., and Zhang, G. (2019). The weather research and forecasting model with aerosol–cloud interactions (wrf-aci): development, evaluation, and initial application. Monthly weather review, 147(5), 1491-1511.

Goudie, A. S. (1978). Dust storms and their geomorphological implications. Journal of Arid Environments, 1(4), 291-311.

Govardhan, G., Nanjundiah, R. S., Satheesh, S. K., Krishnamoorthy, K., and Kotamarthi, V. R. (2015). Performance of WRF-Chem over Indian region: Comparison with measurements. Journal of Earth System Science, 124(4), 875-896.

Govardhan, G., Ambulkar, R., Kulkarni, S., Vishnoi, A., Yadav, P., Choudhury, B. A., ... and Ghude, S. D. (2023). Stubble-burning activities in north-western India in 2021: Contribution to air pollution in Delhi. Heliyon, 9(6).

Govardhan, G., Ghude, S. D., Kumar, R., Sharma, S., Gunwani, P., Jena, C., ... and Rajeevan, M. (2023). Decision Support System version 1.0 (DSS v1. 0) for air quality management in Delhi, India. Geoscientific Model Development Discussions, 2023, 1-30.

Graber, E. R., and Rudich, Y. (2006). Atmospheric HULIS: How humic-like are they? A comprehensive and critical review. Atmospheric Chemistry and Physics, 6(3), 729-753.

Grell, G. A., Peckham, S. E., Schmitz, R., McKeen, S. A., Frost, G., Skamarock, W. C., and Eder, B. (2005). Fully coupled "online" chemistry within the WRF model. Atmospheric environment, 39(37), 6957-6975.

Grell, G. A., and Freitas, S. R. (2014). A scale and aerosol aware stochastic convective parameterization for weather and air quality modeling. Atmospheric Chemistry and Physics, 14(10), 5233-5250.

Guenther, A., Karl, T., Harley, P., Wiedinmyer, C., Palmer, P. I., and Geron, C. (2006). Estimates of global terrestrial isoprene emissions using MEGAN (Model of Emissions of Gases and Aerosols from Nature). Atmospheric Chemistry and Physics, 6(11), 3181-3210.

Han, Y. (2006). JCSDA community radiative transfer model (CRTM): Version 1.

Haywood, J. M., and Shine, K. P. (1995). The effect of anthropogenic sulfate and soot aerosol on the clear sky planetary radiation budget. Geophysical Research Letters, 22(5), 603-606.

Haywood, J., and Boucher, O. (2000). Estimates of the direct and indirect radiative forcing due to tropospheric aerosols: A review. Reviews of geophysics, 38(4), 513-543.

Hersbach, H., Bell, B., Berrisford, P., Hirahara, S., Horányi, A., Muñoz-Sabater, J., ... and Thépaut, J. N. (2020). The ERA5 global reanalysis. Quarterly journal of the royal meteorological society, 146(730), 1999-2049.

https://doi.org/10.5194/egusphere-2026-1100
Preprint. Discussion started: 24 March 2026

Hess, M., Koepke, P., and Schult, I. (1998). Optical properties of aerosols and clouds: The software package OPAC. Bulletin of the American meteorological society, 79(5), 831-844.

Hong, S. Y., and Lim, J. O. J. (2006). The WRF single-moment 6-class microphysics scheme (WSM6). Asia-Pacific Journal of Atmospheric Sciences, 42(2), 129-151.

Iacono, M. J., Delamere, J. S., Mlawer, E. J., Shephard, M. W., Clough, S. A., and Collins, W. D. (2008). Radiative forcing by long-lived greenhouse gases: Calculations with the AER radiative transfer models. Journal of Geophysical Research: Atmospheres, 113(D13).

Janssens-Maenhout, G., Crippa, M., Guizzardi, D., Dentener, F., Muntean, M., Pouliot, G., ... and Li, M. (2015). HTAP_v2. 2: a mosaic of regional and global emission grid maps for 2008 and 2010 to study hemispheric transport of air pollution. Atmospheric Chemistry and Physics, 15(19), 11411-11432.

Jena, C., Ghude, S. D., Kumar, R., Debnath, S., Govardhan, G., Soni, V. K., ... and Rajeevan, M. (2021). Performance of high resolution (400 m) PM2. 5 forecast over Delhi. Scientific reports, 11(1), 4104.

Kanakidou, M., Seinfeld, J. H., Pandis, S. N., Barnes, I., Dentener, F. J., Facchini, M. C., ... and Wilson, J. (2005). Organic aerosol and global climate modelling: a review. Atmospheric Chemistry and Physics, 5(4), 1053-1123.

Kant, S., Kumar, N., and Jenamani, R. K.: Assessment of fog conditions over capital city Delhi (India) during December 2023–January 2024, Nat. Hazards, 1–17, 2025.

Kim, J., Bauer, H., Dobovicnik, T., Hitzenberger, R., Lottin, D., Ferry, D., and Petzold, A. (2012, September). Constraining optical properties and refractive index of soot through combined experimental and modelling studies. In European Aerosol Conference (EAC), Granada, Spain (pp. 2-7).

Kirchstetter, T. W., Novakov, T., and Hobbs, P. V. (2004). Evidence that the spectral dependence of light absorption by aerosols is affected by organic carbon. Journal of Geophysical Research: Atmospheres, 109(D21).

Koven, C. D., and Fung, I. (2006). Inferring dust composition from wavelength-dependent absorption in Aerosol Robotic Network (AERONET) data. Journal of Geophysical Research: Atmospheres, 111(D14).

Kumar, R., Ghude, S. D., Biswas, M., Jena, C., Alessandrini, S., Debnath, S., ... and Rajeevan, M. (2020). Enhancing accuracy of air quality and temperature forecasts during paddy crop residue burning season in Delhi via chemical data assimilation. Journal of Geophysical Research: Atmospheres, 125(17), e2020JD033019.

Kim, D., and Ramanathan, V. (2008). Solar radiation budget and radiative forcing due to aerosols and clouds. Journal of Geophysical Research: Atmospheres, 113(D2).

Lafon, S., Sokolik, I. N., Rajot, J. L., Caquineau, S., and Gaudichet, A. (2006). Characterization of iron oxides in mineral dust aerosols: Implications for light absorption. Journal of Geophysical Research: Atmospheres, 111(D21).

Lettau, H., and Lettau, K. (1969). Shortwave radiation climatonomy. Tellus, 21(2), 209-222.

Li, Z., Guo, J., Ding, A., Liao, H., Liu, J., Sun, Y., ... and Zhu, B. (2017). Aerosol and boundary-layer interactions and impact on air quality. National Science Review, 4(6), 810-833.

https://doi.org/10.5194/egusphere-2026-1100
Preprint. Discussion started: 24 March 2026

Liu, F., Yon, J., Fuentes, A., Lobo, P., Smallwood, G. J., and Corbin, J. C. (2020). Review of recent literature on the light absorption properties of black carbon: Refractive index, mass absorption cross section, and absorption function. Aerosol Science and Technology, 54(1), 33-51.

Mishra, S. K., and Tripathi, S. N. (2008). Modeling optical properties of mineral dust over the Indian Desert. Journal of Geophysical Research: Atmospheres, 113(D23).

Mishra, S. K., Ahlawat, A., Khosla, D., Sharma, C., Prasad, M. V. S. N., Singh, S., ... and Kotnala, R. K. (2018). Experimental investigation of variations in morphology, composition and mixing-state of boundary layer aerosol: A balloon based study over urban environment (New Delhi). Atmospheric Environment, 185, 243-252.

Mlawer, E. J., Taubman, S. J., Brown, P. D., Iacono, M. J., and Clough, S. A. (1997). Radiative transfer for inhomogeneous atmospheres: RRTM, a validated correlated-k model for the longwave. Journal of Geophysical Research: Atmospheres, 102(D14), 16663-16682.

Moteki, N. (2023). Climate-relevant properties of black carbon aerosols revealed by in situ measurements: a review. Progress in Earth and Planetary Science, 10(1), 12.

Nakanishi, M., and Niino, H. (2004). An improved Mellor–Yamada level-3 model with condensation physics: Its design and verification. Boundary-layer meteorology, 112(1), 1-31.

Negi, B. S., Sadasivan, S., Nambi, K. S. V., and Pande, B. M. (1996). Characterization of atmospheric dust at Gurushikar, Mt. Abu, Rajasthan. Environmental monitoring and assessment, 40(3), 253-259.

Negi, B. S., Jha, S. K., Chavan, S. B., Sadasivan, S., Goyal, A., Sapru, M. L., and Bhat, C. L. (2002). Atmospheric dust loads and their elemental composition at a background site in India. Environmental monitoring and assessment, 73(1), 1-6.

Parde, A. N., Ghude, S. D., Sharma, A., Dhangar, N. G., Govardhan, G., Wagh, S., ... and Niyogi, D. (2022). Improving simulation of the fog life cycle with high-resolution land data assimilation: A case study from WiFEX. Atmospheric Research, 278, 106331.

Powers, J. G., Klemp, J. B., Skamarock, W. C., Davis, C. A., Dudhia, J., Gill, D. O., ... and Duda, M. G. (2017). The weather research and forecasting model: Overview, system efforts, and future directions. Bulletin of the American Meteorological Society, 98(8), 1717-1737.

Ramanathan, V. C. P. J., Crutzen, P. J., Kiehl, J. T., and Rosenfeld, D. (2001). Aerosols, climate, and the hydrological cycle. science, 294(5549), 2119-2124.

Ruiz-Arias, J. A., Arbizu-Barrena, C., Santos-Alamillos, F. J., Tovar-Pescador, J., and Pozo-Vázquez, D. (2016). Assessing the surface solar radiation budget in the WRF model: A spatiotemporal analysis of the bias and its causes. Monthly Weather Review, 144(2), 703-711.

Saide, P. E., Spak, S. N., Carmichael, G. R., Mena-Carrasco, M. A., Yang, Q., Howell, S., ... and Springston, S. R. (2012). Evaluating WRF-Chem aerosol indirect effects in Southeast Pacific marine stratocumulus during VOCALS-REx. Atmospheric Chemistry and Physics, 12(6), 3045-3064.

https://doi.org/10.5194/egusphere-2026-1100
Preprint. Discussion started: 24 March 2026

Seinfeld, J. H., and Pandis, S. N. (2016). Atmospheric chemistry and physics: from air pollution to climate change. John Wiley and Sons.

Sengupta, A., Govardhan, G., Debnath, S., Yadav, P., Kulkarni, S. H., Parde, A. N., ... and Ghude, S. D. (2022). Probing into the wintertime meteorology and particulate matter (PM2. 5 and PM10) forecast over Delhi. Atmospheric Pollution Research, 13(6), 101426.

Shettle, E. P., and Fenn, R. W. (1979). Models for the aerosols of the lower atmosphere and the effects of humidity variations on their optical properties (No. 676). Optical Physics Division, Air Force Geophysics Laboratory.

Skamarock, W. C., Klemp, J. B., Dudhia, J. O. G. D., Gill, D. O., Barker, D. M., Duda, M. G., ... and Powers, J. G. (2008). A description of the advanced research WRF Version 3 NCAR. Mesoscale and Microscale Meteorology Division, National Center for Atmospheric Res. Boulder, Colorado, USA, 113.

Skamarock, W. C., Klemp, J. B., Dudhia, J., Gill, D. O., Liu, Z., Berner, J., ... and Huang, X. Y. (2019). A description of the advanced research WRF version 4. NCAR tech. note ncar/tn-556+ str, 145(10.5065).

Sokolik, I. N., and Toon, O. B. (1999). Incorporation of mineralogical composition into models of the radiative properties of mineral aerosol from UV to IR wavelengths. Journal of Geophysical Research: Atmospheres, 104(D8), 9423-9444.

Srivastava, P., Dey, S., Srivastava, A. K., Singh, S., and Tiwari, S. (2018). Most probable mixing state of aerosols in Delhi NCR, northern India. Atmospheric Research, 200, 88-96.

Stier, P., Schutgens, N. A., Bellouin, N., Bian, H., Boucher, O., Chin, M., ... and Zhou, C. (2013). Host model uncertainties in aerosol radiative forcing estimates: results from the AeroCom Prescribed intercomparison study. Atmospheric Chemistry and Physics, 13(6), 3245-3270.

Tomasi, C., Fuzzi, S., and Kokhanovsky, A. (Eds.). (2016). Atmospheric aerosols: life cycles and effects on air quality and climate. John Wiley and Sons.

Toon, O. B., Pollack, J. B., and Khare, B. N. (1976). The optical constants of several atmospheric aerosol species: Ammonium sulfate, aluminum oxide, and sodium chloride. Journal of Geophysical research, 81(33), 5733-5748.

Tuccella, P., Curci, G., Grell, G. A., Visconti, G., Crumeyrolle, S., Schwarzenboeck, A., and Mensah, A. A. (2015). A new chemistry option in WRF-Chem v. 3.4 for the simulation of direct and indirect aerosol effects using VBS: evaluation against IMPACT-EUCAARI data. Geoscientific Model Development, 8(9), 2749-2776.

Twomey, S. (1977). The influence of pollution on the shortwave albedo of clouds. Journal of Atmospheric Sciences, 34(7), 1149-1152.

Wiedinmyer, C., Akagi, S. K., Yokelson, R. J., Emmons, L. K., Al-Saadi, J. A., Orlando, J. J., and Soja, A. J. (2011). The Fire INventory from NCAR (FINN): A high resolution global model to estimate the emissions from open burning. Geoscientific Model Development, 4(3), 625-641.

Wild, M. (2008). Short-wave and long-wave surface radiation budgets in GCMs: a review based on the IPCC-AR4/CMIP3 models. Tellus A: Dynamic Meteorology and Oceanography, 60(5), 932-945.

https://doi.org/10.5194/egusphere-2026-1100
Preprint. Discussion started: 24 March 2026

Yu, H., Liu, S. C., and Dickinson, R. E. (2002). Radiative effects of aerosols on the evolution of the atmospheric boundary layer. Journal of Geophysical Research: Atmospheres, 107(D12), AAC-3.

Zaveri, R. A., Easter, R. C., Fast, J. D., and Peters, L. K. (2008). Model for simulating aerosol interactions and chemistry (MOSAIC). Journal of Geophysical Research: Atmospheres, 113(D13).

Zhang, Y. (2008). Online-coupled meteorology and chemistry models: history, current status, and outlook. Atmospheric Chemistry and Physics, 8(11), 2895-2932.

Zhao, C., Ruby Leung, L., Easter, R., Hand, J., and Avise, J. (2013). Characterization of speciated aerosol direct radiative forcing over California. Journal of Geophysical Research: Atmospheres, 118(5), 2372-2388.